Progress in Neurobiology 264 (2026) 102949

Contents lists available at ScienceDirect

Progress in Neurobiology

journal homepage: www.elsevier.com/locate/pneurobio

Postnatal sensory experience and barrel cortex alterations anticipate autistic traits in a mouse model of CDKL5 deficiency disorder

Alessandra Raspanti [a,1], Riccardo Pizzo [a,1], Antonia Gurgone [a,1,2], Cecilia Giraudo [a], Giulia Sagona [b], Andrea Macioce [a], Anthony Battaglia [a], Lamprini Katsanou [a], Debora Comai [a], Giorgio Medici [c], Francesco Ferrini [d,e], Tommaso Pizzorusso [b,f], Elisabetta Ciani [c], Maurizio Giustetto [a,*]

[a] "Rita Levi-Montalcini" Department of Neuroscience, University of Turin, Turin 10125, Italy
[b] Institute of Neuroscience, National Research Council, Pisa, 56124, Italy
[c] Department of Biomedical and Neuromotor Sciences, University of Bologna, Bologna 40126, Italy
[d] Department of Veterinary Sciences, University of Turin, Grugliasco 10095, Italy
[e] Department of Psychiatry and Neuroscience, Université Laval, Québec, QC, Canada
[f] Scuola Normale Superiore, Biology Laboratory BIO@SNS, Pisa 56124, Italy

ARTICLE INFO

Keywords:
Somatosensory system
Social behaviour
CDKL5 deficiency disorder (CDD)
Barrel cortex
Autism spectrum disorder (ASD)

ABSTRACT

Autistic traits may arise from atypical sensory experience during postnatal life, but whether there is a causal link between defects in cortical circuitry in the brain, altered sensory processing and social behavior remains unknown. Here, we studied tactile stimuli processing in the barrel cortex (BC) and social interactions in juvenile male mice lacking Cyclin-dependent kinase-like 5 (CDKL5), a model of a severe neurodevelopmental disease showing autistic traits and sensory impairments. We identified in these mice defects of whisker-dependent postnatal sensorimotor reflexes, NMDA receptors-dependent signaling, and dendritic orientation in thalamic inputs-receiving spiny stellate neurons. We also found that CDKL5 is required for mapping and processing whisker-derived tactile stimuli in the BC. Intriguingly, KO mice show autistic traits at P21 that are ameliorated by neonatal CDKL5 replacement in the BC. Our data suggest that CDKL5 is required to link tactile processing in the BC to the onset of social interaction abilities.

1. Introduction

The importance of sensory experience in sculpting neuronal connectivity has been widely studied in the past years (Berardi et al., 2004; Hensch, 2005; Hubel and Wiesel, 1970), resulting in the definition of critical periods of brain development when experience shapes neural circuits and strongly affects behavior (Knudsen, 2004). Indirect evidence on the adverse effects of atypical sensory experience throughout neonatal development comes from clinical reports of individuals affected by neurodevelopmental conditions such as autism spectrum disorder (ASD) (Baum et al., 2015; Cheung and Lau, 2020; Patil and Kaple, 2023; Robertson and Baron-Cohen, 2017). Among sensory modalities, somatosensory perception plays a fundamental role in early stages of brain development as it matures before other senses, beginning as early as 8 weeks into gestation, and it can strongly affect motor, cognitive and communication functions (Corbetta and Snapp-Childs, 2009; Hertenstein et al., 2006). Interestingly, aberrant sensorimotor responses have been described in 6-month-old children followed, only in the second year of life, by cognitive and social-communication impairments (Chen and Hong, 2018; Estes et al., 2015), indicating a precise temporal sequence of symptoms in ASD (Boyd et al., 2010; Grzadzinski et al., 2020; Sacrey et al., 2019; Turner-Brown et al., 2013; Wolff et al., 2019). Although early somatosensory alterations are believed to be predictive of autistic traits in adulthood (Estes et al., 2015), the mechanisms hindering the development of somatosensory circuits are still elusive, strongly limiting our understanding of ASD and the development of timely treatment options.

The whisker-mediated touch system in rodents allows tactile

* Correspondence to: Università di Torino, Department of Neuroscience, C.so Raffaello 30, Torino 10125, Italy.
E-mail address: maurizio.giustetto@unito.it (M. Giustetto).
[1] These authors contributed equally.
[2] Present address: Department of Medicine and Surgery, Kore University of Enna, 94100 Enna, Italy

https://doi.org/10.1016/j.pneurobio.2026.102949
Received 27 February 2026; Received in revised form 1 July 2026; Accepted 17 August 2026
Available online 19 August 2026

information to flow from the contralateral thalamus to layer 4 (L4) of the barrel cortex (BC) where thalamocortical axons (TCA) cluster into barrel-like structures, creating a precise cortical topographic map of whiskers in the snout (Erzurumlu and Gaspar, 2020; Vitali and Jabaudon, 2014; Yang et al., 2018). This sensory neuronal network relies on precise wiring during brain development (Staiger and Petersen, 2021) and we and others have shown that mice carrying mutations in ASD-related genes (e.g., Shank3, Fmr1, UBE3A, Cntnap2, Mecp2 and Cdkl5) exhibit tactile abnormalities (Balasco et al., 2022; Bhattacherjee et al., 2017; Chen et al., 2020; Gurgone et al., 2023; Han et al., 2016; He et al., 2017; Orefice et al., 2016; Pizzo et al., 2020). Patients affected by cyclin-dependent kinase-like 5 (CDKL5) deficiency disorder (CDD; OMIM: 300203), a severe neurodevelopmental condition mostly caused by loss-of-function mutations of the X-linked CDKL5 gene, display a broad spectrum of clinical signs, including early-onset epilepsy, impaired psychomotor development, abnormalities in sensory perception, and autistic-like traits (Jakimiec et al., 2020; Van Bergen et al., 2022). We have recently shown that adult Cdkl5 KO mice, together with multiple ASD traits (Jhang et al., 2017), exhibit aberrant whisker-dependent responses that are associated with altered synaptic connectivity and activation of the barrel cortex (Pizzo et al., 2020). Interestingly, CDKL5 expression in mice is elevated at birth, reaching the peak of expression in the cerebral cortex around P14–15 (Rusconi et al., 2008), when the closure of the critical period in the BC occurs (Erzurumlu and Gaspar, 2020; Vitali and Jabaudon, 2014). CDKL5 is a serine/threonine kinase that participates in numerous cellular processes, including gene expression, cell division, neuronal migration, axonal outgrowth, dendritic morphogenesis, and synapse formation (Zhu and Xiong, 2019). Moreover, the identified cytoplasmic targets of CDKL5 phosphorylation (Van Bergen et al., 2022) point to a major role of this kinase in the control of cytoskeletal functions underlying neuronal morphogenesis, including axonal outgrowth and polarization, dendritic branching and spine stability.

All of the above suggests that CDKL5 could contribute early during postnatal development to the sequence of experience-dependent mechanisms regulating BC maturation, tactile information representation, and social behavior. To test this hypothesis, we addressed the early causes underlying aberrant somatosensory perception in Cdkl5 KO mice and searched for the causal relationship with high-order social behavioral deficits. Thus, we investigated the developmental trajectory of sensorimotor responses in Cdkl5 KO mice during the first 15 days of life. We next assessed the integrity of thalamocortical (TC) connectivity, barrel organization, and cortical responses elicited by whisker stimulation in juvenile mutant mice (P15). Finally, we studied the role of CDKL5 on early social behavioral performances and tested the effect of its restricted re-expression in the neonatal BC on the emergence of ASD traits in Cdkl5 KO mice.

2. Materials and methods

2.1. Animals

Animal care and experimental procedures were performed in accordance with European Community Council Directive 86/609/EEC for care and use of experimental animals and with protocols approved by the Italian Minister for Scientific Research (authorization D.M. n∘38/2020-PR 16/1/2020) and the Bioethics Committee of the University of Torino. Generation of the Cdkl5 line has been described previously (Amendola et al.,2014). Experiments were carried out on juvenile (P15-P25) Cdkl5 knockout (KO) male mice. Wild-type (WT) littermates were used for all experiments. After weaning, mice) were housed together with their littermates in groups of 3–4 animals per cage and kept on a regular 12 h light/dark cycle (7:00–19:00 light period) and temperature-controlled environment (21 ± 2°C). Food and water were available ad libitum. To maximally reduce the number of animals used in this study, mice were subjected to multiple behavioural tests, always starting with less invasive ones. All experiments were performed by an operator who was blinded to animal genotype or treatment. Mice were randomly assigned to experimental groups. Exclusion criteria included: aberrant bodyweight, poor coat conditions, and discomfort following surgical and/or behavioural procedures. Although CDD patients are mostly heterozygous girls, we opted to avoid any confounding effects that would derive from analysing heterozygous female mice which express Cdkl5 in a mosaic fashion in about half brain cells. Moreover, being the primary goal of our study to link area-specific contribution of the X-linked gene CDKL5 to brain connectivity, functional responses and behaviour, only CDKL5-null male mice were used in this study.

2.2. Histology and immunofluorescence

2.2.1. Coronal cortical sections

In this study juvenile mice aged between P15-P22 were used. The number of animal used in each experiment is indicated in the result section) were deeply anesthetized by intraperitoneal injection (i.p.) of a mix of tiletamine/zolazepam (40 mg/kg) and xilazine (4–5 mg/kg) and rapidly perfused with phosphate buffered saline (PBS) solution 0.01 M for 2 min, followed by a fixative solution consisting of 4% paraformaldehyde (PFA) in 0.01 M phosphate buffer (PB) for 30 min. The brains were then removed, post-fixed overnight in 4% PFA at 4°C, and subsequently cryoprotected by immersing in 15% and 30% sucrose solution at 4°C. Free-floating 30 μm coronal sections were cut using a cryostat (Leica Biosystems), and stored at −20°C in a cryoprotectant solution containing 30% ethylene glycol and 25% glycerol until use (Pizzo et al., 2016).

2.2.2. Flattened cortex sections

P15 mice were perfused as previously mentioned. Perfused brains were manually splitted in two hemispheres with a razor blade and, by using a small spatula, subcortical structures such as striatum, thalamus and hippocampus were removed to isolate the cortical tissue (Lauer et al., 2018). Subsequently, the resulting hemispheres were placed between two glass slides, filled with 4% PFA, and a weight was placed on top of it in order to make the hemispheres 10–20% thinner than the regular cortices. After 12 h, at 4°C, the flattened cortices were washed (3x10min) with 0.1 M PBS, cryoprotected and cut in 50 μm tangential sections.

2.2.3. Immunohistochemistry and cell analyses

Immunolabelling was conducted as in (Ciccarelli et al., 2013). Briefly, sections were washed three times with 0.01 M PBS (10 min) at room temperature and then permeabilized in 0.01 M PBS solution containing 0.5% Triton X−100 in PBS and 5% normal donkey serum (NDS) for 60 min at room temperature. Subsequently, sections were incubated overnight at 4°C with the following primary antibodies: rabbit anti-Homer1bc (1:500, Synaptic System, 160 023); guinea pig anti-VGluT2 (1:1000, Millipore, 2251); guinea pig anti-VGluT1 (1:1000, Millipore, 5905); rabbit anti-c-fos (1:500, Cell Signaling Technology, 2250S); rabbit anti-GFP (1:1000, Invitrogen, A11122). The following day, sections were washed (3 ×10 min) with 0.01 M PBS and incubated with suitable fluorescent secondary antibodies (1:1000; Jackson ImmunoResearch, West Grove, PA, USA) for 1 h at room temperature. Sections were then washed (3 ×10 min) with 0.01 M PBS, mounted onto glass slides with Dako fluorescence mounting medium (Dako Italia, Italy) and counterstained with the fluorescent nuclear dye DAPI (Sigma-Aldrich). Immunofluorescence images were acquired using a LSM 900 confocal microscope (Zeiss) and images were processed with ImageJ (NIH) or Photoshop CS6 (Adobe Systems). For puncta analysis, stacks of five optical sections (0.5 μm Z- step size) were acquired from L4 BC using a 63X objective (1 Airy unit). Synaptic puncta quantification and juxtaposition was performed by a custom written macro in ImageJ. For c-Fos^{+} cell analysis, stacks of eight optical 1 μm Z- step size) of BC were acquired using a 20X objective. Digital boxes spanning from the pial

surface to the corpus callosum were superimposed at matched locations on each coronal section of the BC and divided into 10 equally sized sampling areas (bins; LI: bin 1; L2/3: bins 2–3; L4: bins 4–5; L5: bins 6–7; L6: bins 8–10). c-Fos$^+$ immunopositive cells in each bin were manually counted as in Gennaccaro et al., (2021), while arbitrary intensity values from c-Fos$^+$ cells were obtained using a dedicated ImageJ tool (integrative density) to analyse Z-stack projected images (Sum value). For c-Fos$^+$ cell analysis following the novelty exposure test, flattened cortices were acquired using a 40X objective. Neurons positive for c-Fos were manually counted within the principal C2 barrel. C-Fos intensity analysis across C2 and adjacent barrels was performed as in Young et al., (2023). In brief, C2-barrel was placed at the center of the image and cropped to include B2 and D2 neighboring barrels. Following background subtraction, a plot profile of pixel intensities across the B2-C2-D2 barrels was generated with the Image J software (NIH, USA). To compare intensity profiles irrespective of genotype-associated differences in c-Fos signal intensity, intensities were binned and normalized to the mean intensity of C2.

2.3. Adeno-associated virus (AAV) injections in the barrel cortex

Intracerebral injection procedures were performed as described by (Kim et al., 2014) with minor changes. Briefly, hypothermic anesthesia of newborn (P0) pups was induced by placement on a cold aluminum foil and kept on ice for 5 min. Proof of anesthesia before injections were the observation of the mouse skin color changing from pink to purple, and the absence of movement after gentle squeezing of the paws. Next, neonatal mice were placed in a stereotaxic neonatal mouse adaptor (Stoelting Co.) and the AAVs delivered using a glass micropipette attached to a nanoliter injector (Nanoject, Dummond Scientific Company) at a rate 23 nL/min. To target L4 of the BC, the following coordinates (in mm, measured from lambda and the pial surface) were used: AP: 1.5; ML: ±1.8; DV: 0.2. For TCA tracing, 50 nl at $1*10^{12}$ viral particles of retrograde AAV-hSyn-EGFP (Addgene 50465-AAVrg) were unilaterally infused. For sparse infection of neurons in the BC, 25 nl of AAV-hSyn-GFP (Addgene 50465-AAV1) at $1*10^{11}$ viral particles were bilaterally injected. For CDKL5 re-expression, 100 nL of a mixture of AAVPHP.B_CDKL5 ($1*10^{12}$ viral particles) and $1*10^{11}$ AAV-hSyn-GFP (Addgene 50465-AAV1) ($1*10^{11}$ viral particles) was bilaterally injected as in Medici et al. (2022). Following injection, pups were placed on a warming pad for at least 10 min before being returned to the home cage.

2.4. Neuronal morphology

To analyze retrogradely labeled TCA bundles, coronal sections were processed for immunofluorescence EGFP-signal amplification using an anti-GFP antibody. Images of the internal capsule and the dorsal striatum were captured from coronal sections using a 20X objective lens. A 100 μm x 100 μm region of interest (ROI) was then selected in the dorsal striatum, and EGFP$^+$ fibers crossing the were manually counted within this area. To exclude the possibility that differences in TCA fluorescence intensity values could depend on unequal viral payloads among animals, we analyzed multiple EGFP stained brain sections for each animal that included both injection site and TCA bundles. TCA fluorescence intensity values were plotted after their normalization with EGFP fluorescence signal intensity in a ROI spanning the AAV injection site in the BC of corresponding sections, and the integrated density of EGFP labeling was calculated using ImageJ software. Moreover, the size of AAV-mediated EGFP expression was measured and expressed as the percentage of BC area labelled by EGFP.

The dendritic polarization analysis of AAV-hSyn-GFP expressing L4 spiny stellate neurons (SSNs) was performed as in Wang et al. (2017). Following GFP signal amplification by immunolabelling with an anti-GFP antibody, images of single SSNs located at the barrel edge were acquired with the confocal microscope in flattened cortices using a 40X objective. Each dendrite was then traced with Image J and their length and arborization pattern was quantified using the orientation bias index (OBI). This index is defined as the ratio of inner dendrite length to total dendrite length. The average OBI of eight SSNs from the same animal was used as the OBI of the animal. Sholl analysis was performed as in Concina et al. (2023). Following dendrites tracing with the NeuronJ Plugin of ImageJ, concentric circles of 10 μm intervals were placed over GFP$^+$ SSNs with the circles center positioned in the middle of the soma. Intersections of different dendritic orders and circles were then counted.

Dendritic spines decorating second order dendritic segments belonging to GFP$^+$ SSN were acquired in tangential sections of flattened cortices with the use of the 40X objective lens of the confocal microscope. Spine number and size were analyzed as in Chapleau et al. (2012) and Concina et al., (2023). Briefly, with ImageJ software both neck-length and head-diameter size were measured manually and employed to calculate neck/head ratios to categorize spine types as follows: mature spines, including mushroom (neck/head ratio < 1) and immature spines (neck/head ratio > 1). Mean spine density was measured as the number of spines per dendritic length unit (μm) with an independent replicate (animal) used as the sampling unit.

2.5. Base scope ISH procedure

CDKL5 mRNA detection was performed as in Medici et al., (2022). Briefly, following PFA perfusion, brains from p25 mice were collected submerged in 4% PFA in 0.01 M PBS for 24 h at 4 °C. Brains were then kept in sucrose solution (30%) at 4°C until sunk. Brains were then cut with a cryostat into 15 μm-thick coronal sections which were serially collected on glasses. The in-situ hybridization (ISH) for the CDKL5 RNA was performed with the Base Scope® technology (Biotechne) following the manufacturer's protocol using a 1ZZ probe designed on the CDKL5 exon 4.

2.6. Immunoblotting

2.6.1. Cortical extract preparation

Mice were sacrificed at P15 by decapitation, and the primary somatosensory cortices were dissected and homogenized in ice-cold RIPA buffer (NP−40 1%, Na deoxycholate 0,25%, EDTA 0.5 M, NaCl 5 M, Tris pH8 1 M, SDS 10%, 1 mM Na-Orthovanadate, 1 mM DTT, 0.5 mM PMSF, 50 mM NaF and protease inhibitors (SIGMAFAST™ Protease Inhibitor Cocktail Tablets, EDTA-Free). The lysates were then centrifuged at 13.000*g* for 20 min at 4°C, the supernatant collected, and protein concentration measured using the BioRad protein assay method (Bio-Rad) (Gurgone et al., 2023).

2.6.2. Synaptosomal fraction preparation

Cortices from juvenile mice were homogenized in ice-cold lysis buffer (0.32 M sucrose, HEPES 1X at pH 7.4, 1 mM EGTA, 1 mM Na-Orthovanadate, 1 mM DTT, phenylmethylsulphonyl fluoride and 1 mM sodium fluoride and protease inhibitors) (SIGMAFAST™ Protease Inhibitor Cocktail Tablets, EDTA-Free), using a glass Teflon tissue grinder. The homogenates were centrifuged at 1000*g* for 10 min at 4°C. After discarding the nuclear pellet, the supernatant was centrifuged at 12,500*g* for 20 min at 4°C. The P1 fraction was then washed with the same initial volume of lysis buffer and underwent further spin (20 min; 12,500 g). The pellet obtained, the crude cortical synaptosomal fraction (P2), was resuspended in 400 μl of RIPA buffer and stored at −80°C. Protein concentration of the synaptosomal fraction was determined with the Bio-Rad protein assay kit (Gurgone et al., 2023).

2.6.3. Western blotting

Proteins (30–50 mg) were mixed with Laemmli buffer 2x (375 mM Tris pH = 6.8, 12%SDS, 60% glycerol, 600 mM DTT, 0.06% bromphenol blue), heated to 90° C for 5 min and then separated on SDS-PAGE gels as in Gurgone et al., (2023). Proteins were transferred to a PVDF membrane. The membranes were blocked for 1 h with BSA 5% or 1% milk in

1x TBS with 1% Tween (TBST) and incubated with the primary antibody overnight at 4°C. After washing (3 ×10 min) with TBST, the membranes were incubated with the appropriate secondary antibody for 1 h at room temperature. For total-protein assessment, the membranes incubated with the phospho-specific primary antibody were stripped with stripping buffer containing 2-mercaptoethanol, 1% SDS, and 62.5 mM Tris-HCl, pH 6.8, at 37°C for 30 min and reprobed with the relative total-protein antibody. The protein amount was normalized relative to the optical density of vinculin or β-actin. The following primary rabbit antibodies were used: NR1 (1:500, Invitrogen, PA5–85751); NR2A (1:1000, Invitrogen, PA5–35377); NR2B (1:1000, Invitrogen, 71–8600); CamKII (1:1000, Millipore, 05–532); pCamKII (1:1000, Abcam, ab34703); AKT (1:1000, Cell Signaling, 4691 P); pAKT (S473) (1:1000, Cell Signaling, 9271); ERK1/2 (1:1000, Cell Signaling, 9194); pERK (T202, T204) (1:1000, Cell Signaling, 4370); CDKL5 (1:500, Atlas Antibodies, HPA002847); β-actin (1:1000, Cell Signaling, 4970); MeCP2 (1:1000, Cell Signaling, 3456); Vinculin (1:1000, Abcam, ab219649). The secondary antibody was a donkey anti-rabbit HRP (1:5000, Thermo Scientific, A16035). The chemiluminescent signal was visualized using Clarity™ Western ECL Blotting Substrates (Bio-Rad) and acquired with Bio-Rad ChemiDocTM Imager (Bio-Rad) and quantified with Image J software (NIH). Protein levels are displayed as fold change.

2.7. Electrophysiology

2.7.1. Slices preparation

Juvenile (P15) mice were anesthetized by inhalation of isoflurane (Merial Italia) and sacrificed by decapitation. The brain was quickly extracted under hypothermic conditions and submerged in ice-cold cutting solution. For slices preparation, the cutting solution was composed of (in mmol/l): 70 sucrose, 80 NaCl, 2.5 KCl, 26 $NaHCO_3$,15 glucose, 7 $MgCl_2$·6 H2O, 1 $CaCl_2$·2 H_2O, 1.25 NaH_2PO_4·H_2O at pH 7.4 by saturation with 95% O_2, 5% CO_2. The region of interest was manually dissected by using a razor blade and blocked on the stage of a Microslicer DTK−1000 vibratome (Dosaka), using cyanoacrylate glue. 350 μm thick coronal slices of S1 cortex, including the barrel field, were cut, maintaining the tissue submerged in an ice-cold solution composed of (in mmol/l): 130 K gluconate, 15 KCl, 20 HEPES, 0.2 EGTA, 11 glucose. Slices were then transferred to a recovery chamber filled with the same solution continuously bubbled with 95% O_2, 5% CO_2, at room temperature (21–22 °C) for at least 1 h before starting the recording. The incubating solution used for the voltage-clamp recordings was composed of (in mmol/l): 125 NaCl, 2.5 KCl, 26 $NaHCO_3$, 15 glucose, 1.3 $MgCl_2$, 2.3 $CaCl_2$·2 H_2O e 1.25 NaH_2PO_4·H_2O.

2.7.2. Voltage-clamp recordings

NMDAR activated currents were recorded in voltage clamp conditions and whole-cell configuration as in Stagni et al., (2017). All electrophysiological recordings of NMDAR-mediated currents were conducted in Layer 4 neurons of the barrel cortex, identified based on their morphology and laminar location in acute coronal slices. Briefly, pyramidal cells were visualized by means of an upright microscope (Axioskop 2 FS; Zeiss, Oberkochen, FRG) equipped with a × 60 water-immersion objective lens, differential-contrast optics, and a near-infrared charge-coupled device (CCD) camera. Slices were perfused with ACSF (continuously bubbled with 95% O_2, 5% CO_2) at a rate of about 1.5 ml/min. Patch pipettes were fabricated from thick-wall borosilicate glass capillaries (CEI GC 150–7.5; Harvard Apparatus, Edenbridge, UK) by means of a Sutter P−87 horizontal puller (Sutter Instruments, Novato, CA, USA). NMDAR-mediated currents were recorded by holding neurons at −70 mV and perfusing them with the NMDAR agonist, N-Methyl-D-aspartate, (NMDA, 50 μM). The external solution contained (in mM): 130 NaCl, 1.8 $CaCl_2$, 10 HEPES, 10 glucose, 1.2 Glycine (pH 7.4). The internal solution contained (in mM): 90 CsCl, 20 TEACl, 10 glucose, 1 MgCl, 4 ATP, 0.5 GTP, 15 phosphocreatine (pH 7.4). These experiments were performed in the presence of the AMPA receptors blockers: 6,7-dinitroquinoxaline−2,3-dione, DNQX (20 μM, Sigma-Aldrich). Tetrodotoxin (TTX 1 μM) was added to block voltage-gated Na^+ channels. Current signals were acquired in gap-free modality with a PC interfaced to a Digidata 1322 A interface (Axon Instruments) using the Clampex program of the pClamp 8.2 software package (Axon Instruments). Current signals were low-pass filtered at 5 kHz and digitized at 20 kHz.

All recordings were performed in the presence of DNQX (20 μM), which specifically blocks non-NMDAR currents (i.e. AMPA/Kainate receptor currents). NMDA was delivered at a submaximal concentration (30 μM) to avoid non-specific effects due to overexcitation (Wirkner et al., 2002, 2007; Hanuska et al., 2024). In some experiments, the selective NMDAR blocker AP5 (50 μM) was applied to assess the specificity of NMDA-induced current.

2.8. Intrinsic optical signal (IOS) imaging

2.8.1. Surgery

The surgery was performed, as previously described in Mazziotti et al., (2017), under isoflurane anesthesia (3% for induction and 1% for maintenance) on juvenile male mice (P22–25). After being placed on a stereotaxic frame and head fixed using ear bars, local anesthesia was provided using subcutaneous lidocaine (2%) injection and eyes were protected with dexamethasone-based ointment (Tobradex, Alcon Novartis). The scalp was removed, and the skull carefully cleaned with saline. Next, a thin layer of cyanoacrylate was poured over the exposed skull to attach a custom-made metal ring (9 mm internal diameter) centered on the barrel cortex. When the glue dried off, a drop of transparent nail polish was spread over the area to ameliorate optical access. During the entire procedure body temperature was controlled using a heating pad and a rectal probe to maintain the animals' body at 37ºC. The animals were left for an hour to recover before the IOS recordings.

2.8.2. IOS recordings

IOS recordings were performed under isoflurane (1%) and chlorprothixene (1.25 mg/Kg, i.p.). Images were obtained using an Olympus microscope (BX50WI) under red light illumination provided by 8 red LEDs (625 nm, Knight Lites KSB1385–1P) attached to the objective (Zeiss Plan-NEOFLUAR 5x, NA 0.16) using a custom-made 3D printed LED holder controlled by an Arduino hardware (Arduino UNO). The animal was secured under the objective using a ring-shaped neodynium magnet (www.supermagnete.it, R−12–09–1.5-N) mounted on an Arduino-based 3D printed imaging chamber that also controls eye shutters and a thermostated heating pad. Visual stimulation was performed using Matlab Psychtoolbox and presented on a monitor placed 13 cm away from the eyes of the mouse: visual stimulus consisted of a sinusoidal wave grating presented in the binocular portion of the visual field with spatial frequency 0.03 cyc/deg, mean luminance 20 cd/m^2 and contrast 90%. The stimulus consisted in the abrupt contrast reversal of a grating with a temporal frequency of 4 Hz for 1 s.

For whisker stimulation, we used piezoelectric bending actuators (PI P−615.30D) connected to a wire custom-made arm touching all whiskers. The stimulus was generated by a sweep generator (Wavetek model 164) connected to an amplifier (E−663 LVPZT-amplifier). Stimuli consisted of 1 mm back-and-forth deflections at 4 Hz for 1 s, on one side of the snout, 0.5 cm away from the face. Frames were acquired at 30 fps, with a resolution of 512 × 512 pixels. A total of 270 frames were captured for each trial: 30 before the stimulus as a baseline condition and 240 as post-stimulus. The signal was averaged for at least 30 trials and down sampled to 10 fps. Fluctuations of reflectance (R) for each pixel were computed as the normalized difference from the average baseline (ΔR/R). For each recording, an image representing the mean evoked response was computed by averaging frames between 0.5 and 2.5 s after stimulation. The mean image was then low-pass filtered with a 2D average spatial filter (30 pixels, 117 μm^2 square kernel). To select the barrel cortex for further analysis, a region of interest (ROI) was

automatically calculated on the mean image of the response by selecting the pixels in the lowest 20% ΔR/R of the range between the maximal and minimal intensity pixel (Cang et al., 2005). To weaken background fluctuations a manually selected polygonal region of reference (ROR) was subtracted. The ROR was placed where no clear response, blood vessel artifact or irregularities of the skull were observed (Heimel et al., 2007). Mean evoked responses were quantitatively estimated as the average intensity inside the ROI.

2.9. Innate sensorimotor reflexes

The examination of the development of motor and sensory performances was carried out from P3 to P15 as described (Arakawa et al., 2015). The analysis of innate reflexes was combined with the investigation of developmental milestones including: eye opening, incision eruption, body weight, and ear detachment. Individual pups were behaviourally tested in the following order: surface righting test, cliff avoidance test, negative geotaxis test, grasp test, whisker stimulation test, and tactile stimulation test.

Surface righting reflex: mice were placed in the supine position, held for 5 s and then released. The latencies required to roll over and have all four paws in contact with the surface were recorded. The maximum time allowed per trial for righting was 60 s. The score was considered absent (0) if the pup lied on its back for 60 s, 1 if it turned in more than 1 s, and 2 if it turned in less than 1 s. Mice were tested in 2 trials for each daily session and the mean score was calculated.

Cliff avoidance test: animals were placed on an edge of elevated platform with both forepaws and nose over the cliff. The mouse's ability to crawl back and turn away from the cliff was scored: (0) pup fell down, (1) pup turned less than 90°, (2) turned 180°. Each pup was tested 2 times in each experimental session, and the mean score was calculated.

Negative geotaxis: pups were placed on an inclined plywood surface (45° angled, 20 ×20 cm) and observed for up to 30 s. The score was considered (0) when pups did not turn around and fell down, (1) $< 90°$, (2) $90° < x < 180°$ turn and (3) 180° turn. Each pup was given 2 trials each test day and the mean score was calculated.

Grasp test: pups were placed in a glass Petri dish, and the experimenter gently applied a little pressure against the palmar surface of a forepaw with a thin rod and the palmar grasp reflex was recorded. This reflex is characterized by closing of the digits in response to an object stroking the palmar surface. The ability to perform this reflex was assigned as: absent (0 points), crooked digits but not grasped (0.5 point), or present (1 point) in each of the forelimbs separately. The score of the grasping reaction was: absent (0 points), grasp but not sustained (0.5 point), or sustained (1 point) in each of the forelimbs separately. Each pup was examined in 2 consecutive trials and the mean of this score was calculated.

Whisker stimulation test: this test was performed to assess behavioral reaction, such as twitching responses and head moving reactions, after unilateral whiskers stimulation with a thin stainless-steel rod (0.5 mm in diameter) for 20 s without touching the inter-vibrissal fur or the snout skin. A score of 1 was assigned when a reaction was shown, and 0 when it was absent.

Tactile stimulation test: pups were kept in a glass Petri dish for 1 min, following the whisker stimulation test, and several points along the body, including the top of the head, medial back, left and right forepaws, hind paws, and the base of the tail (total 7 points) were manually poked 5 times with a thin stainless-steel rod (0.5 mm diameter). The reaction of mice, for each stimulated part of the body, was measured. A score of 1 was assigned when a reaction was shown, and 0 when it was absent.

2.10. ASD-related behavioral tests

The behavioral studies were carried out in the morning on mice aged P21–25. Mice were habituated to the test room for at least 1 h before each test and the behavior tests housing cleaned between each trial with 70% ethanol.

Open field test: exploratory behavior in a novel environment was assessed by a 20 min session within an open field arena (50 cm (L) x 50 cm (W) x 40 cm (H)) made of gray Plexiglas. Juvenile mice (P21–25) were placed in the center of the arena and then the videorecording using a digital camera was started. Locomotor activity (distance traveled and speed, resting time) in the entire arena were then analyzed using the Smart 3.0 software (Panlab) (Gurgone et al., 2023).

Juvenile play test: juvenile social interactions were assessed in 21–22 day-old pairs of male mice from different litters as previously described (Tărlungeanu et al., 2016). Prior to the social interaction session, mice were individually housed for 1 h in a standard laboratory cage, without access to food and water. After an hour of individualized housing, each mouse was placed alone in the play testing cage for a 10-min habituation period. The floor of the arena was covered with a thin and fresh layer (0.5 cm) of the same type of bedding that is used for the home cage. After mice were habituated, a pair of animals of the same sex was placed simultaneously in the testing arena and video recording immediately started. Two genotype combinations were assessed: WT/WT and KO/KO mice. Mice were recorded for the initial 10 min, when social interaction is active. Behavioral activities including anogenital sniffing, nose-to-nose sniffing, body sniffing, push crawl and follow, were manually evaluated by an investigator blinded to the genotypes.

Repetitive behavior: mice were individually placed into a clean home-cage like environment lined with bedding. After 5 min of habituation, 10 min of activity was recorded. The number of repetitive behaviours, defined as grooming, digging and jumping was scored manually using a stopwatch as described in Baronio et al., (2015).

2.11. Novelty exposure test

This test was performed in P21 Cdkl5 and WT littermates. The day before the experiment, mice were habituated to the testing room and arena. Afterwards, all the whiskers of the snout were completely trimmed except the C2 whisker on the left whisker pad. The day after, the mouse was placed in the testing arena filled with objects with different textures. Mice were free to investigate novel objects for 1 h while their track was recorded. Immediately after, mice were perfused, the hemisphere flattened, and the tissue processed for c-Fos staining as described in Antón-Bolaños et al. (2019).

2.12. Statistics

Statistical analysis was performed using Prism software (Graphpad). Statistical values including the n, statistical test and significance are reported in the figure legends. The data were analyzed by: (i) one- or two-way analysis of variance (ANOVA) followed by the Bonferroni test, if differences were found; (ii) unpaired *t*-test; (iii) Mann–Whitney test. All data are reported as mean ± SEM and considered to be statistically significant when $p < 0.05$. In each graph circles/dots represent individual values. From all analyses, outlier samples were excluded according to the "identify outliers" function (Method: ROUT, Q= 2%) present in Prism software. Sample size was determined using G*Power software 3.1.9.2 (RRID:SCR_013726) by setting power at 0.8 and significance level (α) = 0,05 for all the experiments. Sample size for each experiment was calculated based on the specific statistical test employed for the analysis. For histological and behavioural analyses sample size indicates number of animals whereas for electrophysiological investigations the sample size indicates the number of slices.

3. Results

3.1. Aberrant onset and development of sensorimotor responses in Cdkl5 KO pups

To assess the developmental trajectory of sensorimotor integration

processes in mice lacking Cdkl5, we performed a battery of tests dependent on whisker-mediated sensorimotor responses from P3 to P15. To this aim, both Cdkl5 KO and WT littermates were evaluated in the execution of innate motor behaviors: surface righting, negative geotaxis and grasping reflexes (Arakawa and Erzurumlu, 2015; Sullivan et al., 2003) (Supplementary Fig. 1A-C).

Surface righting. Cdkl5 KO mice did not show significant differences compared to control littermates in the latency to turn to a prone position (2-way ANOVA Genotype F (1, 245) = 1.795, $p > 0.05$; Supplementary Fig. 1 A).

Negative geotaxis. This test evaluates both vestibular and body coordination by assessing the ability of pups to reorient themselves towards an upwards position when placed on a downward incline. Pups lacking Cdkl5 displayed a marked inability in this test compared to WT littermates (2-way ANOVA Genotype F (1, 243) = 14.98, $p < 0.001$; Supplementary Fig.1B), a sign that was particularly apparent at P15 as highlighted by Bonferroni's multiple comparison analysis ($p < 0.001$).

Grasping reflexes. This test evaluates both the onset of the grasping reflex and the strength of the paw. Although the grasp reflex was detectable already at P3 in both genotypes (Supplementary Fig. 1 C), the developmental trajectory was atypical in Cdkl5 KO mice compared to WT pups until P12 (2-way ANOVA Genotype F (1, 243) = 18.99, $p < 0.001$, Bonferroni post-hoc test: $p < 0.001$ P9; $p < 0.05$ P12) (Zafeiriou, 2004).

Whisker stimulation. The repetitive presentations of unilateral whisker stimulation generate in rodent pups a startle response resulting in horizontal head movements, head-up, face or snout twitching (Arakawa and Erzurumlu, 2015; Sullivan et al., 2003). Interestingly, the mild deflection of mystacial vibrissae produced clear motor responses in both WT and Cdkl5 KO pups; however, the developmental score of these physical reactions was higher in KO mice compared to WT littermates as highlighted by 2-way ANOVA (Genotype F (1, 220) = 1.982, $p < 0.05$; Supplementary Fig. 1D), with no significant differences shown by the ages analyzed.

Tactile stimulation. We evaluated the writhe response to the gentle application of a tactile stimulus to different body areas including head, back, tail, and the four paws. A strong difference was seen in Cdkl5 KO pups compared to WT littermates (2-way ANOVA Genotype F (1, 245) = 13.49, $p < 0.001$), specifically at P15 (Bonferroni post-hoc test $p < 0.001$; Supplementary Fig. 1E) (Hertenstein et al., 2006).

Cliff avoidance. This test relies on the mice's inherent response to turn away from a cliff. We observed a significant impairment of Cdkl5 KO mice to avoid the cliff compared to WT littermates (2-way ANOVA Genotype F (1, 234) = 24.22, $p < 0.001$) (Supplementary Fig. 1 F) at both P9 and P12 (Bonferroni post-hoc test $p < 0.01$) (Geuze, 2003).

Finally, we assessed if atypical sensorimotor responses shown by Cdkl5 KO pups were associated with changes in physical developmental landmarks. Body weight growth did not differ between genotypes until P15 (2-way ANOVA Genotype F (1161) = 6.82, $p < 0.001$; age F (3161) = 282.3, $p < 0.001$), when a slight, but significant, decrease was observed in mutant pups. Moreover, no temporal differences in eye opening, incisor eruption, and ear detachment were present between genotypes (Supplementary Fig. 1 G) (Fong et al., 2012; Goddard-Blythe, 2000, 2011). Altogether, these results suggest that the lack of CDKL5 severely affects the physical responses underlying sensorimotor integration in early stages of life development.

3.2. Early disruption of cortical activation, NMDA-mediated neurotransmission and intracellular signaling in the BC of juvenile Cdkl5 KO mice

Tactile sensorimotor integration in neonatal mice critically relies on the anatomical and functional integrity of the BC (Petersen, 2019). Unstimulated Cdkl5 KO and WT littermate mice were sacrificed under resting conditions, having been maintained in their home-cage environment without exposure to novel stimuli or handling beyond routine care, to assess basal levels of neuronal activation. We found several molecular and neuronal alterations affecting this cortical area in P15 Cdkl5 KO mice.

Our experiments show a significant reduction of c-Fos$^+$ cell density, an indicator of neuronal activation, in Cdkl5 KO mice compared to WT littermates (2-way ANOVA Genotype F (1, 102) = 12.81, $p < 0.001$; Fig. 1A). Interestingly, post-hoc statistical analyses revealed a selective decrease of c-Fos immunoreactivity in L4 (Bonferroni post-hoc test: L4 $p < 0.01$). However, genotype did not significantly influence c-Fos intensity (F (1,17) = 1.94, $p = 0.182$), and the interaction between genotype and layer was also not significant (F (5,85) = 1.43, $p = 0.223$). These results suggest that while overall neuronal activation, as measured by c-Fos$^+$ cell density, is reduced in Cdkl5 KO mice, the relative c-Fos protein levels per active neuron are not significantly altered across layers or genotypes.

Next, we used whole-cell patch-clamp recordings on P15 BC slices to test N-methyl-D-aspartate (NMDA)-mediated excitatory neurotransmission, as it plays a fundamental role in the development and plasticity of rodent somatosensory cortex (Mizuno et al., 2021). The application of 30 μM NMDA produced an inward current (I_{NMDA}) in both WT and Cdkl5 KO BC pyramidal neurons (Fig. 1B). As we previously observed in Cdkl5 KO cortical neuronal cultures (Gurgone et al., 2023), I_{NMDA} was significantly lower in Cdkl5 KO mice compared to WT littermates (WT: 822.7.4 ± 171.4.3 pA; KO: 391.2 ± 65.3 pA; unpaired *t*-test $p < 0.05$; Fig. 1B). Importantly, the application of the selective NMDAR blocker AP5 (50 μM) prevented the NMDA-induced slow currents and thus confirmed their specificity.

We next analyzed the expression levels of NR2A and NR2B subunits in cortical extracts of WT and Cdkl5 KO juvenile mice (Fig. 1C). We found no differences in NR1 levels, the constitutive subunit of NMDAR, between WT and Cdkl5 KO (unpaired *t*-test $p = 0.39$; Fig. 1D). In contrast, the expression of both NR2A and NR2B, the major regulatory subunits differentially expressed during BC development, were significantly lower in Cdkl5 KO cortical extracts (NR2A: unpaired *t*-test $p < 0.05$; NR2B: unpaired *t*-test $p < 0.05$; Fig. 1E, F) (Tang et al., 2019). Finally, we analyzed NMDAR-mediated postsynaptic signaling (Krapivinsky et al., 2003; Lisman et al., 2012; Wang et al., 2012; Giese, 2021) by evaluating the levels of the phosphorylated forms of $Ca2^+$/Calmodulin-dependent kinase II (CaMKII), AKT and ERK in cortical synaptosomal extracts (Fig. 1G). As shown in Fig. 1H and I, we found a significant reduction in the levels of p-CaMKII (unpaired *t*-test $p < 0.05$) and p-AKT (S473) (unpaired *t*-test $p < 0.05$) in P15 Cdkl5 KO mice compared to WT littermates, whereas pERK did not show significant differences (Fig. 1J). No changes were detected in the total form of these proteins between genotypes (Fig. 1H-J). The efficiency of synaptosomes purification was validated by assessing that the nuclear protein MeCP2 was present only in the total cortical homogenate while absent from the P2 fraction (Supplementary Fig. 3) (Rusconi et al., 2008). Altogether these data indicate that neuronal activation, NMDAR-mediated excitatory neurotransmission, and postsynaptic intracellular pathways are impaired in the BC of juvenile Cdkl5 KO mice and suggest that these alterations crucially contribute to the onset of sensorimotor deficits.

3.3. The loss of Cdkl5 interferes with dendritic asymmetry of L4 spiny stellate cells

The establishment of TC wiring requires NMDARs-mediated neurotransmission (Iwasato et al., 2000), which we have found altered in the BC of Cdkl5 KO mice. Because spiny stellate neurons (SSNs) in L4 are the main recipient of TC inputs, relaying tactile information from whiskers in the snout to the BC (Feldmeyer, 2012), we assessed the integrity of their morphology and connectivity.

To this aim, AAV-mediated retrograde labeling of TCA was obtained by injections in the BC of both WT and KO mice. Confocal microscopy images of fluorescent axons were captured in an area corresponding to

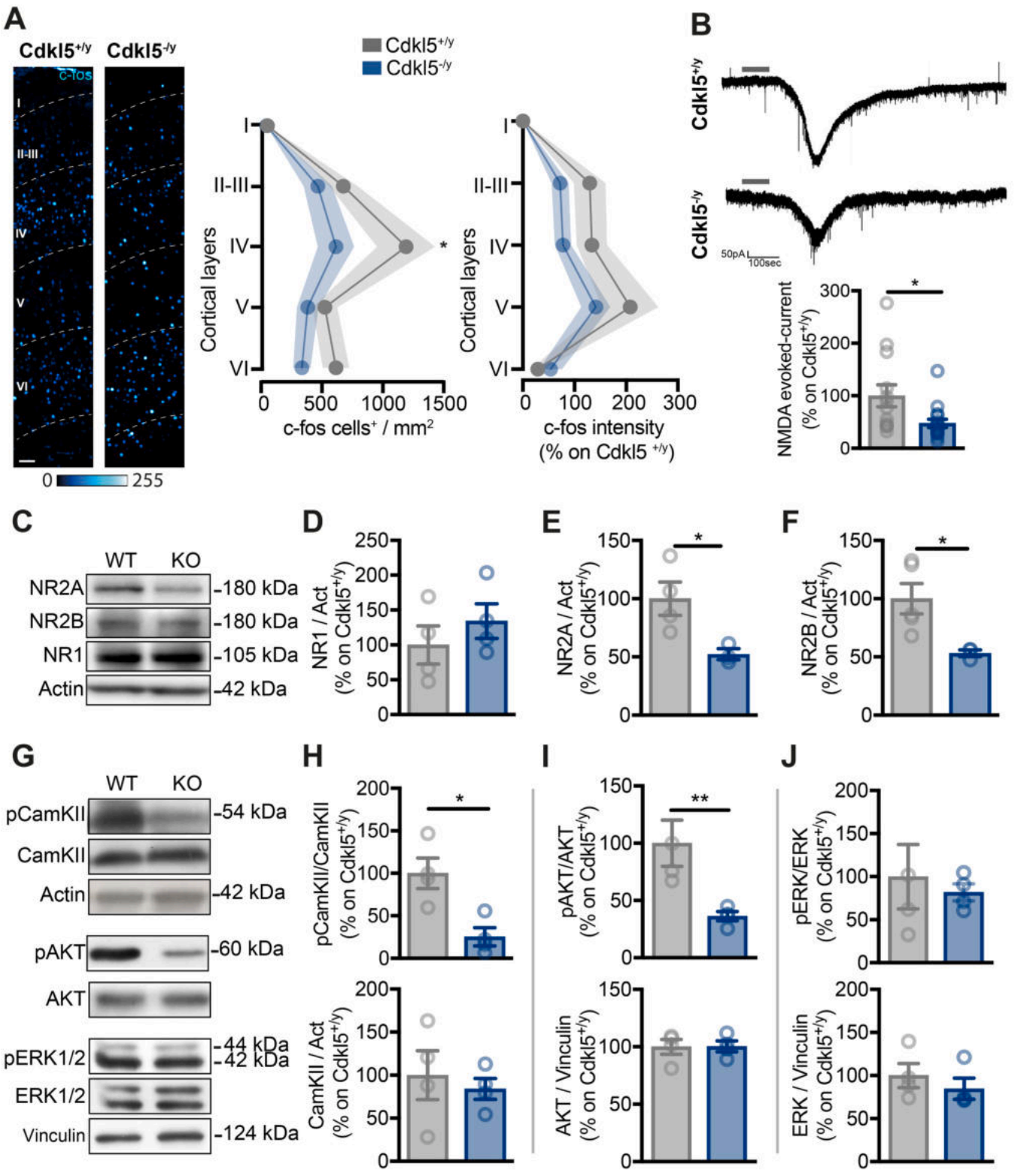

Fig. 1. Aberrant NMDAR function, expression and dependent pathways are associated with decreased BC neuronal activation in P15 juvenile Cdkl5$^{-/y}$ mice. (A) Representative c-Fos^{+} immunofluorescence confocal images in the BC of Cdkl5$^{+/y}$ and Cdkl5$^{-/y}$ mice at P15 (Scale bar 50 um) and quantification of c-Fos^{+} cells density and intensity throughout cortical layers (Cdkl5$^{+/y}$ = 10; 9 Cdkl5$^{-/y}$ = 9). (B) NMDA-mediated current traces and histogram showing inward current (I_{NMDA}) amplitude recorded in acute S1 slices of juvenile Cdkl5$^{-/y}$ mice and Cdkl5$^{+/y}$ littermates following bath application of 30 μM NMDA (grey line) (cells: 13 Cdkl5$^{-/y}$; 16 Cdkl5$^{+/y}$). (C) Representative western blots of NR1, NR2A and NR2B in cortical extracts of Cdkl5$^{+/y}$ and Cdkl5$^{-/y}$ mice at postnatal at P15 and graphs showing the quantitative analysis of the total protein levels for NR1 (D), NR2A (E) and NR2B (F) levels normalized to actin (Cdkl5$^{+/y}$ = 4; Cdkl5$^{-/y}$= 4/3). (G) Representative western blots of pCamKII, CamKII, pERK1/2, ERK1/2, pAKT, AKT and housekeeping proteins (actin and vinculin) in synaptosomal extracts of Cdkl5$^{+/y}$ and Cdkl5$^{-/y}$ mice at P15. Quantitative analyses revealed a significant reduction of pCamKII/CamKII ratio in Cdkl5$^{-/y}$ mice (H), as well as for the pAKT/AKT ratio (I) whereas no differences were identified for in pERK1/2 (J). Statistical analyses: *t*-test, 2-way ANOVA followed by Bonferroni post-hoc test *p < 0.05, **p < 0.01.

the dorsal striatum of P15 mice (Fig. 2A-B). Interestingly, TCA organization did not reveal substantial differences in axonal density between WT and Cdkl5 KO mice (unpaired *t*-test $p < 0.05$; Fig. 2C). To exclude any difference due to AAV infection, we normalized TCA density values on the mean EGFP intensity shown by the injection site in the BC. As shown in Fig. 2D, also after this normalization no differences were found between genotypes, thus suggesting the integrity of TCA extension is preserved in juvenile Cdkl5 KO mice. Importantly, also when the infected area of the BC showing AAV-mediated EGFP expression was measured, no differences between groups of animals were found (Supplementary Fig. 4).

Finally, we assessed the intensity of EGFP-expression in TCA across the area of interest (dashed area in Fig. 2B). This analysis revealed a general reduction of TCA fluorescence in KO mice, suggesting that lack of Cdkl5 may alter either retrograde transport mechanisms or axonal size (2-way ANOVA Genotype $F(1, 6264) = 398.7$, $p < 0.001$; Fig. 2E). To exclude major anatomical abnormalities of the thalamic VPM nucleus, we assessed its cellular density (Supplementary Fig. 5). The count of $DAPI^+$ cells present in this nucleus revealed no difference between genotypes.

Next, we studied the morphology of SSNs, the postsynaptic targets of TCA inputs. Barrels form in the first week after birth once they are reached by presynaptic TCA contacting L4 SSNs that are localized at barrel edges and become polarized by extending dendrites asymmetrically toward barrel hollow upon receiving TCA inputs (Li and Crair, 2011; Wang et al., 2017; Wu et al., 2011).

Thus, we assessed the role of CDKL5 on SSNs polarity by investigating the dendritic organization of sparsely-labeled GFP^+ SSNs in tangential sections of flattened cortices of mice injected with AAV-hSyn-GFP in the BC at p0 (Fig. 2F) (Mazziotti et al., 2017). GFP^+ neurons, whose cell bodies were located at barrel edges (Fig. 2F', G), were selected and the orientation bias index (OBI) of their dendrites, i.e., the ratio of the length of hollow-projecting dendrites to the total dendrite length, was determined.

Intriguingly, whereas in WT mice SSNs extended most dendrites toward the hollow, Cdkl5 KO SSNs showed numerous dendritic segments oriented into the septa (Fig. 2G). This qualitative observation was confirmed by quantitative evaluation of both OBI (unpaired *t*-test $p < 0.05$) and total dendritic length, measured in barrel hollows and septa (2-way ANOVA followed by Bonferroni, hollow vs septa, WT $p < 0.001$, KO $p = 0.08$; Fig. 2H, I). The atypical orientation shown by Cdkl5 KO SSNs did not result from abnormal dendritic growth as the total dendritic length was similar between genotypes (unpaired *t*-test $p = 0.92$; Fig. 2J).

To characterize whether the loss of CDKL5 might also impact the branching complexity of SNNs dendrites, we conducted a Sholl analysis. As shown in Fig. 2K, the 2-way ANOVA revealed a statistically significant difference between genotypes ($p < 0.001$) with the KO SSNs showing a reduced number of intersections compared to WT cells. We previously demonstrated that CDKL5 is required for dendritic spine maturation and stabilization in cortical excitatory neurons within the S1 cortex (Della Sala et al., 2016), in agreement with findings reported by Terzic et al. (2021) in the hippocampus. Given the hierarchical organization of sensory inputs processing in the BC, with SSNs being the primary postsynaptic target of TCA (Feldmeyer, 2012), we assessed dendritic spines structure decorating these neurons. We found that the density of dendritic spines protruding from secondary dendrites of GFP^+ SSNs did not differ between genotypes (Fig. 2L, M). In contrast, when we evaluated their morphology, 2-way ANOVA revealed a genotype x spine category (i.e. mature vs. immature) interaction ($F(1, 10) = 5.31$, $p < 0.05$), although Bonferroni post-hoc test did not detect significant differences between genotypes (immature: $p = 0.73$, mature: $p = 0.059$; Fig. 2N). On the other hand, cumulative distribution of spine density based on neck/head ratio values confirmed these structural alterations by revealing a statistically significant difference (Mann-Whitney, $p < 0.001$; Fig. 2O).

Thus, these data indicate that Cdkl5 loss produces an atypical orientation of SSNs dendrites and alters the maturation of the dendritic spines decorating these cells. These findings show that Cdkl5 loss, while it seems to only mildly affect TCA growth and path-finding into the BC, produces severe morphological alterations in L4 SSNs that can underlie abnormal thalamocortical connectivity.

3.4. *Cdkl5 KO mice show early atypical TC connectivity in L4 of the BC*

Tangential sections through L4 of the BC were immunostained with an antiserum against the vesicular glutamate transporter 2 (VGluT2), to selectively label TCA terminals (Pizzo et al., 2020; Terzic et al., 2021). Although the outline of TCA in the posteromedial barrel subfield, where mystacial vibrissae are represented, did not show any substantial difference between genotypes (Fig. 3A), a significant decrease of VGluT2 immunofluorescence was observed in Cdkl5 KO mice compared to WT littermates (unpaired *t*-test $p < 0.05$; Fig. 3B), indicative of altered synaptic integrity. In agreement with this, we found a robust reduction in the density (Fig. 3C, D), size (Fig. 3E), and fluorescence intensity (Fig. 3G) of $VGluT2^+$ puncta in Cdkl5 KO mice compared with WT littermates (unpaired *t*-test $p < 0.001$). In addition, Cdkl5 null mice showed lower density of VGluT2-$Homer1bc^+$ puncta appositions (unpaired *t*-test $p < 0.001$), resulting in a greater number of postsynaptic spines lacking an identifiable thalamic input (Fig. 3F). Interestingly, both density and size of $Homer1bc^+$ puncta did not differ between genotypes (unpaired *t*-test $p > 0.05$; Fig. 3H, I). SSNs in L4 make recurrent excitatory intracortical connections with neighboring SSNs that are needed to amplify cortical activation during sensory stimulation (Staiger and Petersen, 2021). We found that in Cdkl5 KO mice the integrity of such intracortical connectivity, which is identified by anti-VGluT1 immunostaining, was preserved. Both the density of $VGluT1^+$ puncta and VGluT1-$Homer^+$ juxtapositions (unpaired *t*-test $p > 0.05$; Fig. 3L) were unaffected in Cdkl5 KO mice compared to WT littermates (Fig. 3J, K), whereas $VGluT1^+$ puncta size was slightly decreased (Fig. 3M). These results indicate that at this developmental stage, by affecting the growth of TCA presynaptic terminals, the lack of CDKL5 interferes with the formation and/or stabilization of axospinous thalamocortical synapses in L4 of the BC.

3.5. *Enhanced cortical response to whisker stimulation in juvenile Cdkl5 KO mice*

To functionally assess sensory information processing within the BC, we examined whisker-evoked responses using intact skull intrinsic optical signal (IOS) imaging of the BC in juvenile animals (Fig. 4A) (Mazziotti et al., 2017). Fig. 4B shows typical examples of responses consisting of a decrease in reflectance (darker area) induced by tactile stimulation in the BC.

Data quantitation showed that mechanical stimulation of the contralateral mystical vibrissae produced similar amplitudes of the responses in the two genotypes (unpaired *t*-test $p = 0.12$; Fig. 4C).

To elucidate whether the BC hyperactivation might be associated with an altered segregation of whisker-mediated inputs into corresponding L4 receptive fields, we employed the novelty exposure test (Antón-Bolaños et al., 2019). Briefly, P21 Cdkl5 KO and WT littermates were habituated to the test environment the day before the experiment. All whiskers were trimmed except the left C2 whisker. The following day, mice freely explored a textured-object arena for one hour. Immediately after the session, brains were collected to assess c-Fos expression in the C2 barrel, corresponding to the stimulated vibrissa, to evaluate sensory-dependent neuronal responses in the somatosensory cortex (Fig. 4D). In agreement with the IOS results, we observed an increase in c-Fos intensity in the BC area corresponding to the remaining C2 whisker (unpaired *t*-test, $p < 0.05$; Fig. 4E, G), as well as a trend toward an increase in the density of c-Fos^+ cells (unpaired *t*-test, $p = 0.11$; Fig. 4F).

To determine whether whisker-related information was confined to

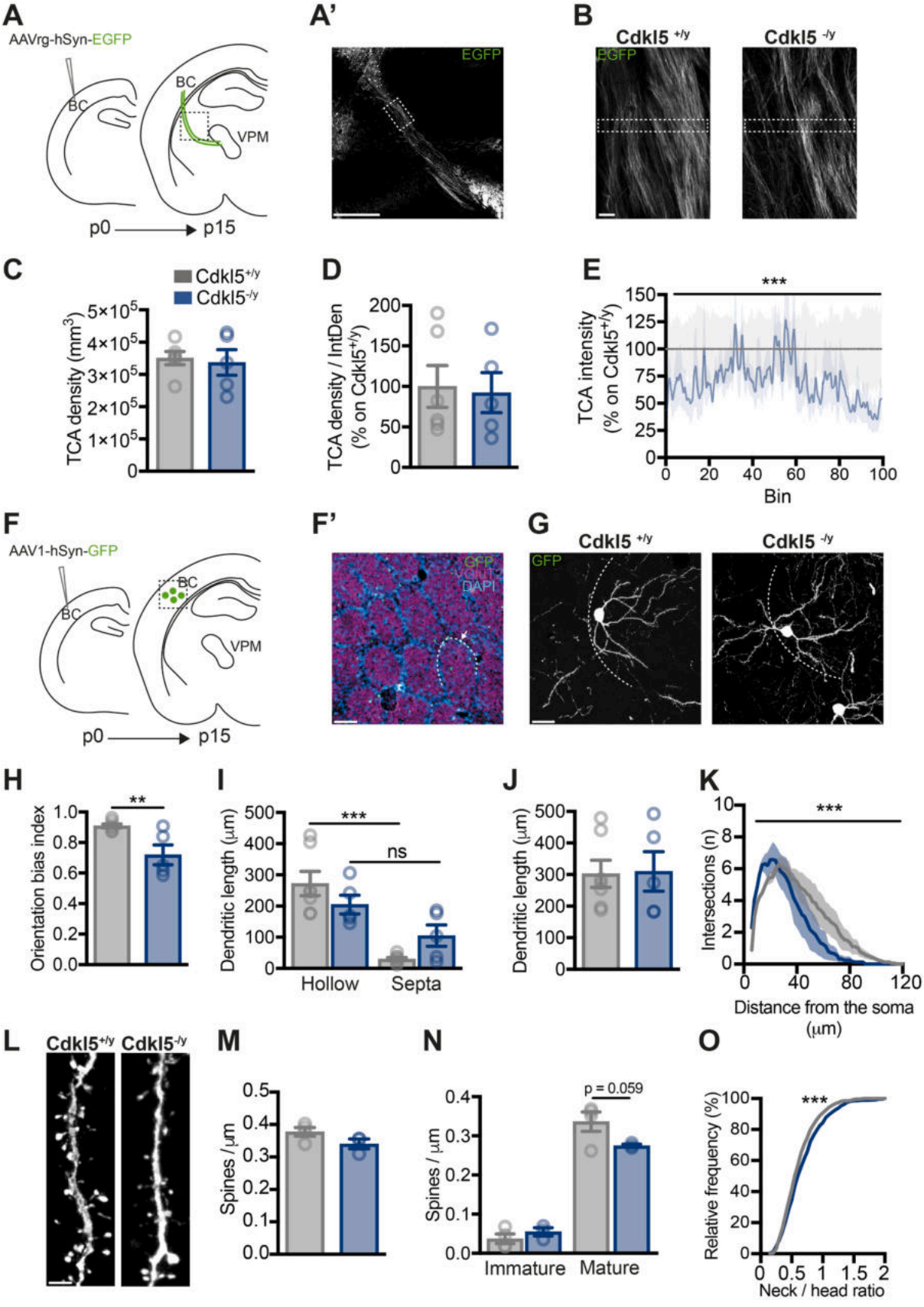

(caption on next page)

Fig. 2. Cdkl5 loss impacts typical dendritic asymmetry of L4 spiny stellate cells. (A) Schematic illustrating stereotaxic AAVrg-hSyn-EGFP injections into the BC of P0 Cdkl5$^{+/y}$ and Cdkl5$^{-/y}$ mice to label TC projections to BC and (A') confocal micrograph showing labeled TCAs of P14 mice in the boxed area in panel A corresponding to the dorsal striatum. (B) Higher magnification confocal images of the outlined area in panel A' in P14 Cdkl5$^{+/y}$ and Cdkl5$^{-/y}$ mice. (C, D) The analysis of the density of individual EGFP^{+} TCAs (C) and the TCAs density corrected on the mean intensity of the injection site in the BC (D) did not reveal any significant differences between Cdkl5$^{+/y}$ and Cdkl5$^{-/y}$ mice. (E) The analysis of the TCA intensity quantified in the area enclosed by the dashed line in B shows a reduction in the Cdkl5$^{-/y}$ mice suggesting a decreased TCA diameter. (F) Schematic representation of the sparse stereotaxic AAV-hSyn-GFP injections into the BC of P0 Cdkl5$^{+/y}$ and Cdkl5$^{-/y}$ mice to label spiny stellate cells (SSNs) and (F') confocal micrograph on tangential sections of flattened cortices showing labeled SSNs in L4 BC (boxed area in panel F) identified by VGluT2 staining in P15 mice. Arrow indicates a L4 SSN whose soma is located in the barrel wall (dotted line). (G) Higher magnification confocal images of flattened cortices showing GFP^{+} L4 SSN of P15 Cdkl5$^{+/y}$ and Cdkl5$^{-/y}$ mice located in the barrel wall (dotted line). (H-J) The orientation bias index (H) (i.e. the ratio of the hollow projecting dendritic length to total dendritic length) was significantly decreased in Cdkl5$^{-/y}$ SSNs; Cdkl5$^{-/y}$ SSNs showed a trend towards a decrease in hollow-projecting dendritic length and a trend towards an increase in septa-projecting dendritic length (I). (J) Total dendritic length is unchanged in Cdkl5$^{-/y}$ SSNs. (K) The Sholl analysis of SSN dendritic branching revealed a reduced number of intersections in Cdkl5$^{-/y}$ in comparison to Cdkl5$^{+/y}$ (Cdkl5$^{+/y}$ = 5; Cdkl5$^{-/y}$ = 4; 6 SSNs/animal). (L) Micrographs depicting secondary dendrites from Cdkl5$^{+/y}$ and Cdkl5$^{-/y}$ SSNs. (M) No statistically significant differences in dendritic spine density were observed in Cdkl5$^{-/y}$ compared to Cdkl5$^{+/y}$ mice. (N) A trend towards reduction was found in the density of mature dendritic spines in Cdkl5$^{-/y}$ compared to Cdkl5$^{+/y}$ SSNs (N); cumulative analysis of spine density based on neck/head ratio showed a statistically significant decrease between the 2 experimental groups (O) (Cdkl5$^{+/y}$ = 4; Cdkl5$^{-/y}$ = 3; 5 SSNs / animal; 2 secondary dendrites / SSN). Scale bars: A', F' 100 μm; B, G 20 μm; L, 2 μm. Statistical analysis: *t*-test, 2 way-ANOVA, Bonferroni's post hoc test, Mann-Whitney, ** $p < 0.01$, *** $p < 0.001$.

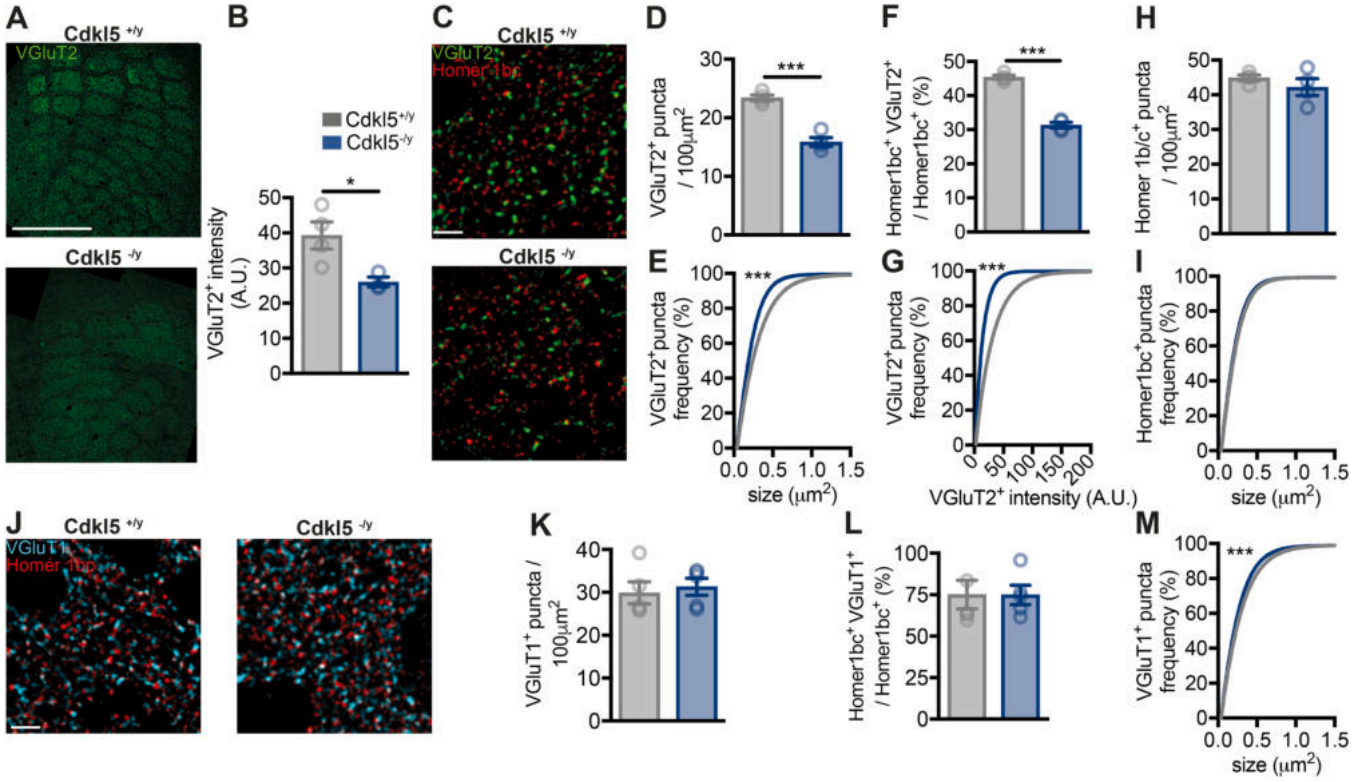

Fig. 3. Cdkl5 loss induces circuit-specific defects of L4 barrel cortex connectivity in juvenile Cdkl5$^{-/y}$ mice. (A) Representative VGluT2 immunofluorescence of tangential sections through L4 revealing the organization of thalamo-cortical (TC) afferents in the BC of both Cdkl5$^{+/y}$ and Cdkl5$^{-/y}$ mice (scale bar 500 μm) and (B) histogram showing the analysis of VGluT2^{+} staining intensity (n = 4). (C) Micrographs showing TC synapses in L4 of the BC from Cdkl5$^{+/y}$ and Cdkl5$^{-/y}$ mutants (scale bar 5 μm). (D-G) Quantification of VGluT2^{+} TC inputs density (D), size (E), intensity (G) and the percentage of VGluT2^{+} TC afferents juxtaposed to a Homer1bc^{+} puncta (F) (n = 4) revealed a strong impairment of TC synapses in the Cdkl5$^{-/y}$ mice compared to Cdkl5$^{+/y}$ littermates. (H, I) No overall changes in either the density or the size of Homer1bc^{+} dendritic spine were identified. (J) Micrographs showing the cortico-cortical (CC) synapses in L4 of the BC from Cdkl5$^{+/y}$ and Cdkl5$^{-/y}$ mutants (scale bar 5 μm). (K-M) Quantification of the density of VGluT1^{+} puncta (K) as well as the percentage of VGluT1^{+} afferents juxtaposed to a Homer1bc^{+} puncta (L) revealed no overall changes in the number of intra-cortical excitatory terminals between Cdkl5$^{+/y}$ and Cdkl5$^{-/y}$. Nevertheless, mutants exhibit a slight decrease in the VGluT1^{+} puncta size (M) (Cdkl5$^{+/y}$ = 4; Cdkl5$^{-/y}$ = 5). Statistical analysis: *t*-test, Mann-Whitney, *$p < 0.05$, *** $p < 0.001$.

its corresponding cortical barrel in Cdkl5 KO mice, we analyzed c-Fos immunofluorescence in the C2 and neighboring barrels (boxed areas in Fig. 4E) (Young et al., 2023). The intensity distribution analysis revealed that in Cdkl5 KO mice the c-Fos immunosignal was not restricted to the intact C2-whisker barrel, but instead appeared more widespread in adjacent barrel regions compared to WT animals (2-way ANOVA Genotype: $F(1, 2000) = 35.80$, $p < 0.001$; Fig. 4H). These findings indicate that Cdkl5 KO mice exhibit sensory-driven hyperactivation of the BC that is paralleled by altered mapping of whisker activity.

3.6. Autism-like behaviors appear early in Cdkl5 KO mice

Early tactile stimulation and experience during development are essential for brain maturation, cognition, and adult social behaviors (Hertenstein et al., 2006; Mikkelsen et al., 2018; Orefice et al., 2016, 2019). To assess whether the alterations in sensorimotor responses, TC connectivity, and BC activation produced by the lack of Cdkl5 are associated with the emergence of ASD-like signs, we performed a behavioral tests (i.e., juvenile play and repetitive behavior) from P21 to P25, a developmental time window when the first social interactions

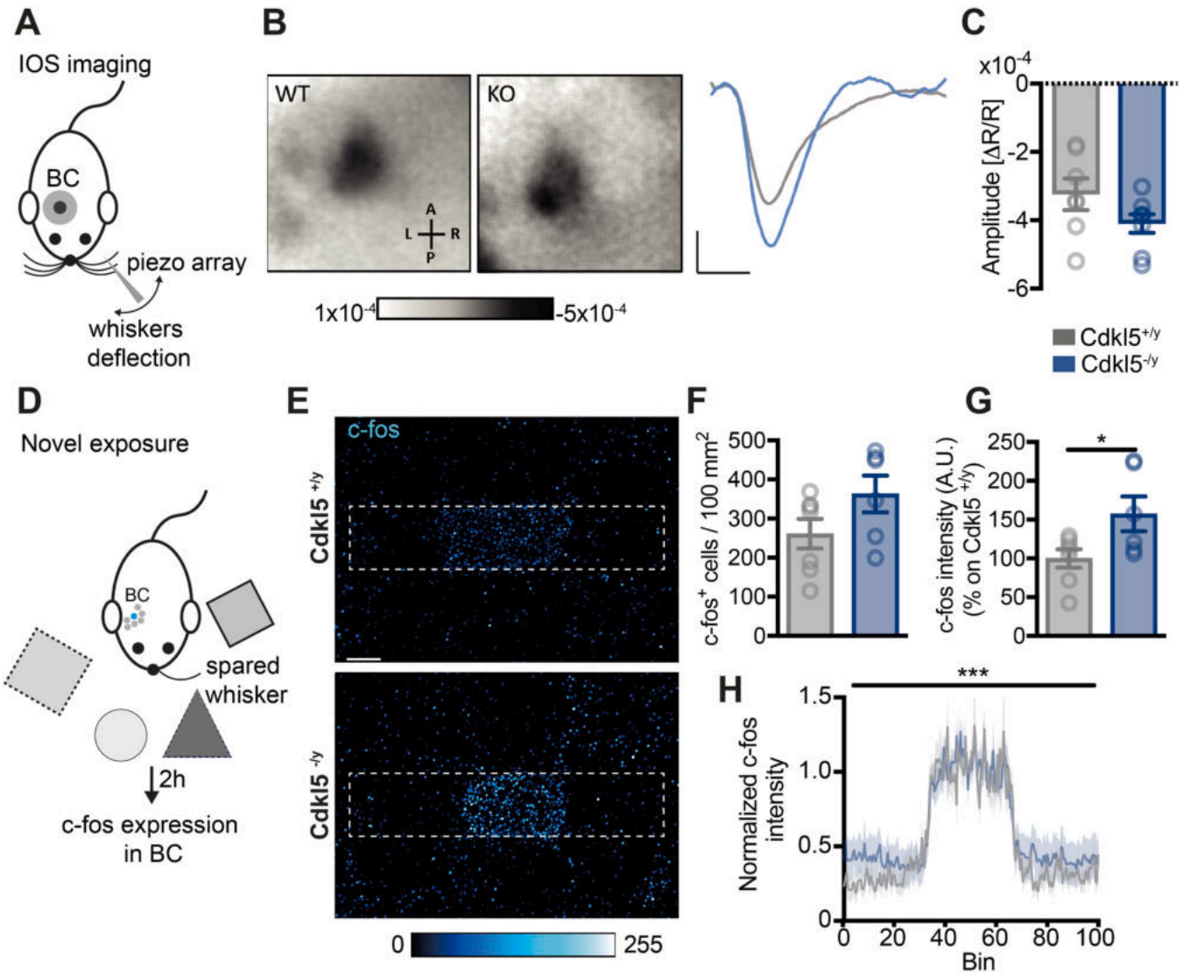

Fig. 4. Cdkl5$^{-/y}$ mice show aberrant cortical response following whisker stimulation. (A) Schematic of the experimental setup of the intrinsic optical imaging (IOS). 4 Hz whiskers deflection in the left whisker pad was produced by using a piezo-motor based stimulator. (B) Responsive area of contralateral BC of Cdkl5$^{+/y}$ and Cdkl5$^{-/y}$ mice after whisker stimulation and related traces. (C) Quantification of IOS amplitude revealed an increased responsiveness of BC in Cdkl5$^{-/y}$ mice despite not reaching the significance ($p = 0.12$) (Cdkl5$^{+/y}$ = 7; Cdkl5$^{-/y}$ = 8). (D) Schematic for the novelty exposure paradigm for assessing whisker-dependent neuronal activity. Mice were cut all but the C2 whisker and then placed in a novel texture environment. Whisker-evoked activity in the barrel cortex was assessed 2 h after novelty exposure by c-Fos$^+$ expression. (E) Representative images of tangential sections for c-Fos$^+$ immunofluorescence intensity in the C2 barrel of Cdkl5$^{+/y}$ and Cdkl5$^{-/y}$ mice subjected to the novelty exposure paradigm. (F, G) Quantification histograms of c-Fos$^+$ cells density and intensity in the corresponding C2 barrel showed, in the mutant mice, cortical hyperactivation as indicated by the trend toward increase of c-Fos$^+$ cells (F) and the significant increase in c-Fos$^+$ intensity (G). (H) Graph showing the profiles of c-Fos$^+$ expression intensity across the ROIs outlined in (E); c-Fos$^+$ intensity is normalized to the peak C2 barrel intensity (Cdkl5$^{+/y}$ = 7; Cdkl5$^{-/y}$ = 8). Scale bar: 100 μm. Statistical analyses: *t*-test, 2-way ANOVA *$p < 0.05$, ***$p < 0.001$.

between conspecifics occur (Tărlungeanu et al., 2016).

First, we used an established same-sex dyadic interaction paradigm employed to evaluate social behavior in mice from P21, namely the juvenile play test (McFarlane et al., 2008). Intriguingly, in this test Cdkl5 KO pairs displayed significantly reduced interactions compared to WT pairs (unpaired *t*-test $p < 0.05$; Fig. 5A).

To exclude that impaired locomotion contributes to the atypical social behavior displayed by Cdkl5 KO mice, we performed the open field test. As shown in Fig. 5D-G, juvenile KO mice exhibited increased exploratory behavior, higher mean speed, and a marked reduction in resting time (unpaired *t*-test $p < 0.01$), indicating that enhanced exploratory behavior, which we and others have previously reported in adult Cdkl5 KO mice (Jhang et al., 2017; Wang et al., 2012; Terzic et al., 2021; Song et al., 2025; Amendola et al., 2014), is already detectable during early developmental stages.

Finally, we assessed repetitive behaviors, another core feature of ASDs, in juvenile mice in a home-cage environment. Cdkl5 KO mice showed a significantly reduced time engaged in stereotypic behaviors such as jumping and digging compared to littermate controls (unpaired *t*-test $p < 0.05$; Fig. 5B, C). Altogether, these data indicate that Cdkl5 KO mice exhibit early-onset atypical spontaneous social interactions compared to WT littermates, confirming that defective morpho-functional organization of the BC is paralleled by the emergence of autistic-like behaviors.

3.7. Neonatal correction of Cdkl5 expression in the BC alleviates ASD-like behaviors

To address whether the onset of ASD-like traits in Cdkl5 KO mice is directly caused by abnormalities affecting BC connectivity and

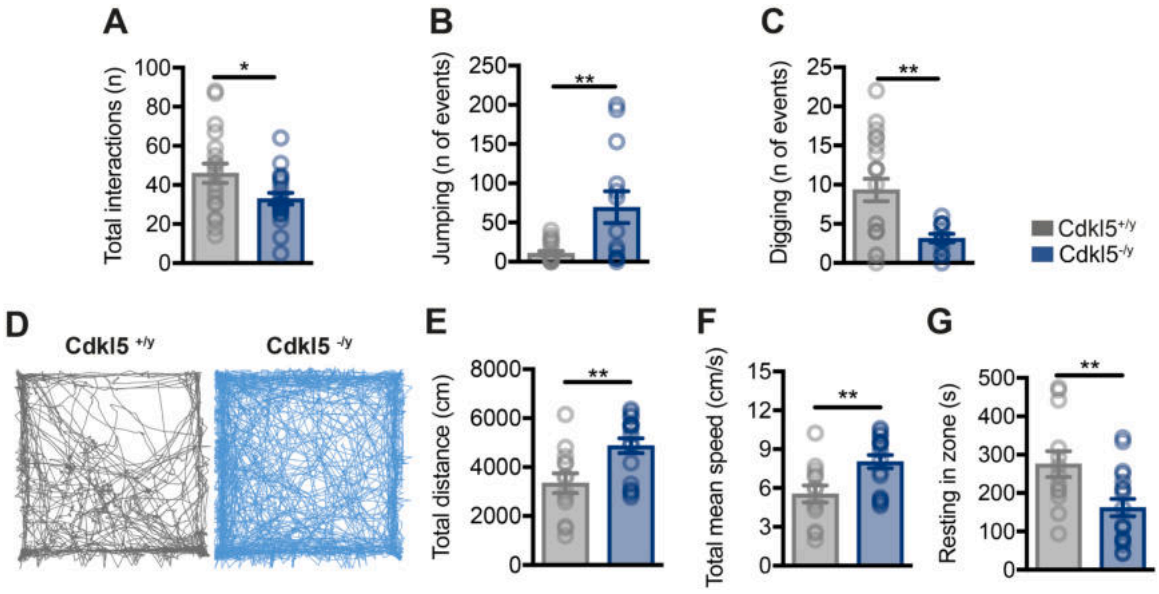

Fig. 5. Juvenile P21-P25 Cdkl5$^{-/y}$ mice show autistic-like phenotypes. (A) Quantification of the reciprocal social interaction events (nose-to-nose interaction, body sniffing, anogenital sniffing, follow, push-crawl) which showed a reduction in Cdkl5$^{-/y}$ pairs compared to Cdkl5$^{+/y}$ pairs (Cdkl5$^{+/y}$ = 14; Cdkl5$^{-/y}$ = 16). (B, C) Abnormal stereotypical behaviors in juvenile Cdkl5$^{-/y}$ mice as revealed by the number of jumping (B) and digging (C) events (Cdkl5$^{+/y}$ = 12; Cdkl5$^{-/y}$ = 10). (D-G) Increased explorative behavior in juvenile Cdkl5$^{-/y}$ mice is evaluated by the open field test. (D) Representative trajectories and quantification of (E) total distance moved, (F) speed and (G) total resting time pointed out an early hyperactivity of Cdkl5$^{-/y}$ mice compared to Cdkl5$^{+/y}$ littermates (Cdkl5$^{+/y}$ = 13; Cdkl5$^{-/y}$ = 18). Statistical analyses: *t*-test, 2-way ANOVA followed by Bonferroni's post hoc test, *p < 0.05 **p < 0.01 ***p < 0.001.

responsiveness, we evaluated whether Cdkl5 re-expression in the BC, using a gene replacement strategy (Medici et al., 2022), could rescue ASD-like deficits. To this aim, the AAVPHP.B_CDKL5 vector or vehicle was bilaterally administered into the BC of Cdkl5 KO and WT mice, respectively, at P0 (Fig. 6A). To visualize injection sites and confirm the consistency of AAV targeting to the BC, AAVPHP.B_CDKL5 or vehicle preparations were supplemented with diluted AAV-hSyn-GFP to enable sparse neuronal labeling (Supplementary Fig. 6). Mice were tested for social and repetitive behaviors 24 days after injection. In agreement with our observations in untreated mice, vehicle-injected Cdkl5 KO pairs exhibited a significant decrease in social interaction events compared to WT mice (1-way ANOVA, Fisher's LSD post-hoc test; WT-vehicle vs KO-vehicle, p < 0.05; Fig. 6B). Remarkably, restoration of CDKL5 expression mainly in the BC resulted in a robust improvement of atypical social behavior, as indicated by the number of spontaneous social interactions displayed by AAVPHP.B_CDKL5-injected Cdkl5 KO mice

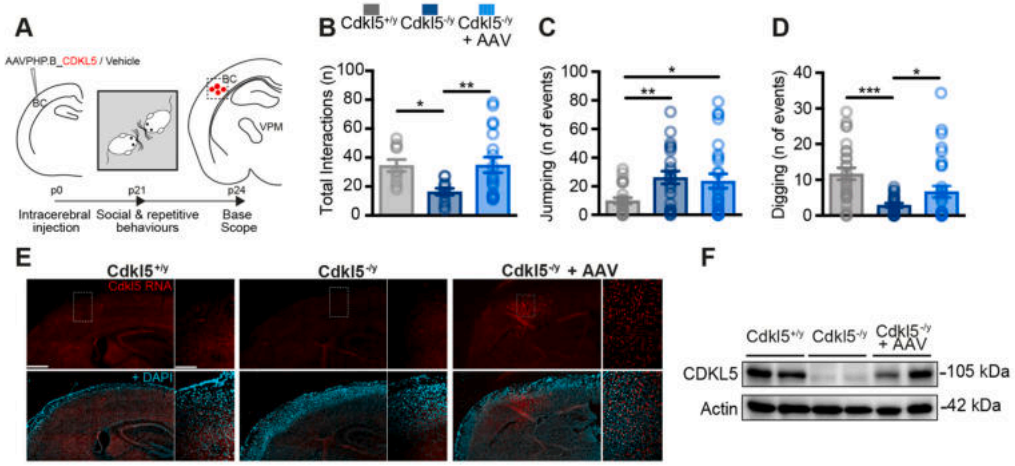

Fig. 6. Neonatal CDKL5 expression in KO mutants reverts ASD-like symptoms in juvenile mice. (A) Schematic representation of neonatal CDKL5 re-expression. Mice underwent bilateral injection with AAVPHP.B_CDKL5, at a dose of $1*10^{12}$ (100nL), in BC at P0. Mice were tested for both social and repetitive behaviours 3 weeks later; finally, brains were collected for analysing CDKL5 re-expression by RNAScope. (B) Restored levels of social behavior in juvenile Cdkl5$^{-/y}$ mice 3 weeks after AAV9 injection as indicated by the analysis of the number of direct interactions (vehicle injected Cdkl5$^{+/y}$ = 24; vehicle injected Cdkl5$^{-/y}$ = 18; AAV injected Cdkl5$^{-/y}$ = 19). (C, D) Impact of CDKL5 re-expression on stereotypical behaviours exhibited by Cdkl5$^{-/y}$ mice. No significant effects were observed in the jumping events (C) whereas digging impairments were completely corrected by AAV injection (D). (E) Representative confocal images of CDKL5 mRNA detected by RNA Scope in the BC of Cdkl5$^{+/y}$ and Cdkl5$^{-/y}$ mice injected with vehicle, and of Cdkl5$^{-/y}$ mice injected with the AAVPHP.B_CDKL5 vector. The dotted areas outline the BC and are shown as higher magnification panels. Sections are counterstained with DAPI. Scale bars: 30 μm. (F) Representative Western blot showing CDKL5 expression in Cdkl5$^{+/y}$ and Cdkl5$^{-/y}$ mice injected with vehicle, and in Cdkl5$^{-/y}$ mice injected with AAVPHP.B_CDKL5. Each lane represents an individual sample. Actin was used as a loading control. Statistical analysis: 1-way ANOVA followed by Sidak post-hoc test: *p < 0.05 **p < 0.01 ***p < 0.001.

(1-way ANOVA, Fisher's LSD post-hoc test; KO-vehicle vs KO-AAV, $p < 0.01$; Fig. 6B). In contrast, CDKL5 re-expression led to a partial improvement of repetitive behaviors (Fig. 6C, D). Vehicle-injected KO mice displayed abnormal jumping (1-way ANOVA, Fisher's LSD post-hoc test; WT-vehicle vs KO-vehicle, $p < 0.01$) and digging phenotypes (1-way ANOVA, Fisher's LSD post-hoc test; WT-vehicle vs KO-vehicle, $p < 0.01$), consistent with our previous findings (Fig. 5E, F). While AAVPHP.B_CDKL5 injection had no significant effect on the number of jumping events (1-way ANOVA, Fisher's LSD post-hoc test; KO-vehicle vs KO-AAV, $p = 0.67$; WT-vehicle vs KO-AAV, $p < 0.05$; Fig. 6C), restoration of CDKL5 expression in the BC rescued digging behavior in Cdkl5 KO mice (1-way ANOVA, Fisher's LSD post-hoc test; KO-vehicle vs KO-AAV, $p < 0.05$; WT-vehicle vs KO-AAV, $p = 0.07$; Fig. 6D).

To confirm the efficiency of gene transfer mediated by AAVPHP.B_CDKL5, expression was assessed by fluorescence in situ hybridization using a probe targeting CDKL5 exon 4 (Tassinari et al., 2023). As shown in Fig. 6E, CDKL5 mRNA re-expression was primarily confined to the BC, though not exclusively.

To further verify CDKL5 protein restoration following AAVPHP.B_CDKL5 injection, the BC was dissected, and protein lysates were analyzed by Western blotting to detect CDKL5 expression. As shown in Fig. 6F, clear re-expression of CDKL5 protein was observed in AAVPHP.B_CDKL5-injected Cdkl5 KO mice, albeit at lower levels than in WT cortices, whereas no signal was detected in cortical samples from vehicle-injected Cdkl5 KO animals. These results confirm the efficacy of the viral vector in restoring CDKL5 expression in the BC of KO animals.

Altogether, these data indicate that early correction of Cdkl5 expression in the BC of Cdkl5 KO mice alleviates early-onset spontaneous social interaction deficits and partially rescues stereotypic behaviors, thereby revealing a causal link between CDKL5 function in the BC and the emergence of autistic-like behaviors.

4. Discussion

The ability to plan and execute an appropriate motor response to environmental demands is based on the proper development of the nervous system, through which innate sensorimotor reflexes, elicitable in humans within the first six months of life (Zafeiriou, 2004), are progressively inhibited and replaced by postural reflexes (Geuze, 2003; Fong et al., 2012). If primary reflexes persist beyond the typical developmental time frame, they can interfere with maturation processes and diminish the brain's capacity to process sensory information efficiently (Goddard-Blythe, 2000, 2011; Parfrey et al., 2014).

With this study, we provide evidence that mice lacking CDKL5 show a delay in the disappearance of innate sensorimotor reflexes, especially those based on whisker-BC mediated processing (i.e., negative geotaxis test and tactile stimulation reflex), remaining present at P15. This observation aligns with recent findings showing that certain reflexes persist beyond the typical developmental timeline in children with ASD, while others do not emerge when expected (Teitelbaum et al., 2004) and supports the idea of monitoring sensorimotor reflexes as early autism biomarkers.

Such behavioral development is accompanied by the formation of the barrel system in the S1 cortex, that is responsible for whisker-dependent sensorimotor control and devised as an integrated and refined network connecting whiskers, thalamus, and cortex. Indeed, we show for the first time that CDKL5 is required for the early developmental processes shaping the organization of the BC. First, we show that the reduced efficacy of NMDA-mediated transmission in the BC of juvenile Cdkl5 KO mice produces alterations in signaling pathways (i.e., CaMKII and AKT) crucial for the formation, maintenance and plasticity of synaptic connectivity (Kennedy, 2013). Moreover, the number of c-Fos$^+$ cells in L4 are robustly reduced in the BC of Cdkl5 KO mice at P15, indicating that abnormal cortical activation shown by adult KO mice (Gurgone et al., 2023; Pizzo et al., 2020; Tassinari et al., 2023) originates early.

Intriguingly, our data disclose that CDKL5 positively regulates NMDAR expression and function during the critical developmental periods for whisker map formation. By showing that both INMDA and expression of NR2A and NR2B subunits are reduced in the absence of CDKL5 starting from P15, these experiments are in agreement with our previous data obtained in primary cultures of S1 neurons from Cdkl5 KO mice (Gurgone et al., 2023). Although previous studies investigated the involvement of CDKL5 in NMDAR function, no conclusive evidence is available. In a full KO mouse model, CDKL5 loss was accompanied by defective NR2B amount in hippocampal PSD fraction (Okuda et al., 2017; Tang et al., 2019; Terzic et al., 2021), whereas no changes were detected in both hippocampal and cortical membrane-bound levels of NR2A and NR2B in a Cdkl5 KI (R59X) model (Yennawar et al., 2019). The most parsimonious explanation of these differences arises from either the CDKL5 mouse model used or the cellular fractions investigated in these studies.

Consistently with our current findings, previous studies show that cortex-specific deletion of NMDAR subunits tampers with the integrity of BC organization and SSNs dendritic orientation (Datwani et al., 2002; Iwasato et al., 2000; Mizuno et al., 2014), cellular signs that we report in Cdkl5 KO animals. In addition, metabotropic glutamate receptor 5 (mGluR5) activity was shown to cell-autonomously regulate SSNs polarization and the coordinated dendritic outgrowth toward TCA (Ballester-Rosado et al., 2016; Huang and Lu, 2018). Because we recently showed that CDKL5 loss reduces mGluR5 expression and function in the S1 cortex (Gurgone et al., 2023), our current results prompt further studies assessing the role of this glutamatergic receptor class in the alterations of the barrel system produced by the lack of CDKL5.

Barrel map formation is the result of a coordinated crosstalk between presynaptic TC inputs and L4 SSNs (Narboux-Nême et al., 2012; Vitalis et al., 2018), a circuit that we show to be severely affected in juvenile Cdkl5 KO animals. Our data show that the reduced number of TCA presynaptic boutons unlikely depends on differences in cellular density in the VPM nucleus nor to major alterations of TCA, beside a slight decrease of their retrograde transport efficiency.

In contrast, we found that SSNs dendrites in L4, which must receive highly organized TC inputs to promote tactile sensory processing in the BC (Petersen, 2019), show profound defects of their arborization and polarization in juvenile Cdkl5 KO mice, defects that can be caused by the recognized defects of microtubule-dependent anterograde trafficking in dendrites lacking CDKL5 (Baltussen et al., 2018). Moreover, in line both with our previous observation in S1 of adult Cdkl5 KO mice (Della Sala et al., 2016) and with the role of CDKL5 in the postsynaptic compartment, we found that the maturation of spines decorating SSNs dendrites is defective in juvenile Cdkl5 KO mice. It is thus possible to conceive that such altered dendritic spine structure contributes to the reduction of TC synaptic contact that we report in L4 of the BC in Cdkl5 KO mice.

We disclose for the first time that mapping of tactile stimuli in the BC is aberrant in juvenile Cdkl5 KO, a defect that parallels atypical tactile responses shown by these animals during the first 15 postnatal days. Despite a highly disorganized and dysfunctional BC, the magnitude of evoked responses in awake juvenile Cdkl5 KO mice was exaggerated and not segregated within the limits of the corresponding C2 barrel when single-whisker deflection was applied. Interestingly, the orientation of SSNs dendritic processes toward the barrel hollow is necessary for bifacial cortical mapping of whisker representation. In contrast, abnormal dendritic polarization in SSNs, as we observed in Cdkl5 mutants, results in impaired whisker stimuli segregation that leads to overlap with responses from neighboring whiskers (Nakagawa and Iwasato, 2023; Wang et al., 2017).

Thus, our data provide first evidence that an ASD-related gene is important early during development for the morphological requirements of SSNs to promote correct cortical mapping of sensory stimuli. Moreover, although further studies are needed to clarify how

the connectivity defects we found in juvenile Cdkl5 KO mice result in hypoactivation of the BC at resting conditions and hyperactivation following whisker stimulation, it is feasible to hypothesize that early-onset dysfunctional tuning of sensory inputs leads to maladaptations in adult Cdkl5 mutant mice which will no longer show typical responses to sensory stimulation. Our current findings, which appear in contrast with previous studies showing that cortical responses are reduced in adult Cdkl5 KO mice (Gurgone et al., 2023; Lupori et al., 2019; Mazziotti et al., 2017; Pizzo et al., 2020), add novel information on the developmental trajectory of dysfunctional sensory tuning in Cdkl5 mutants.

We found significant alterations of social behaviour in juvenile Cdkl5 KO mice starting from P21, a time when interaction with conspecifics begins (Tărlungeanu et al., 2016), and that such early-onset atypical social responses were associated with autistic traits, such as repetitive or stereotyped behaviors (i.e., digging and jumping), as previously observed in adult Cdkl5 KO mice (Pizzo et al., 2020; Tang et al., 2019; Vigli et al., 2019; Jhang et al., 2017). Because early cortical dysfunction leading to irregularities in tactile perception can in turn adversely affect behavioral responses (Riemersma et al., 2024), we anticipated that the alterations in the BC of juvenile Cdkl5 KO mice promote early defects in social interactions and autistic traits shown by these mutants.

Intriguingly, neonatal replacement with a functional copy of CDKL5 restricted to the BC partially improved both social behavior and autistic traits in Cdkl5 mutant mice, suggesting a potential causal link between aberrant development of the whisker-to-barrel circuit and early-onset autistic-like behavior in Cdkl5 KO mice. Although the contribution of thalamic circuits remains to be clarified in future studies, our findings are consistent with an early role of CDKL5 within BC circuitry for somatosensory and tactile perception, sociability, and ASD-like behaviors. Thus, our data together with previous evidence strongly argue that further studies addressing the molecular mechanisms regulating the developmental maturation BC shall be sought to better understand its role in the autistic traits associated with CDD, also in view of the development of therapeutic strategies.

Interestingly, our study offers new insights about the functions of CDKL5 by disclosing a new role of this kinase in the critical period of developmental BC plasticity (Erzurumlu and Gaspar, 2012). To further address CDKL5 function in neurodevelopment, and consequently the causes underlying the limited reversibility of atypical behaviours in older mutant mice (Song et al., 2025), it will be crucial to explore later intervention time points, such as re-expressing CDKL5 right before or after the closure of the multiple critical periods of plasticity described in the BC (Erzurumlu and Gaspar, 2020). However, our data anticipate that the re-expression of CDKL5 in the BC after the closure of experience-dependent structural critical period (P5-P7; Erzurumlu and Gaspar, 2012; 2020) would be ineffective, or less efficient, in rescuing the behavioural and social responses we found ameliorated in early treated animals. In this regard, an intervention provided later than the abnormal EEG transition period (P10-P12) identified by Liao and collaborators (Liao and Lee, 2023). in CDKL5-deficient mice may also result in a less efficient rescue. These authors have suggested that developmentally regulated genes may represent key pathogenic substrates underlying neonatal epilepsy, strongly suggesting that early CDKL5 expression is needed to establish typical neuronal excitability and connectivity in the developing BC.

In sum, understanding the mechanisms through which ASD-related genes operate during crucial developmental periods, as we have pursued in this study, can foster comprehension of autism-related aberrant sensory processing and improve temporal tuning of personalized intervention strategies in affected individuals.

CRediT authorship contribution statement

Anthony Battaglia: Investigation. **Andrea Macioce:** Investigation. **Giulia Sagona:** Methodology, Investigation, Formal analysis, Data curation. **Cecilia Giraudo:** Investigation. **Maurizio Giustetto:** Writing – original draft, Supervision, Project administration, Funding acquisition, Formal analysis, Data curation, Conceptualization. **Antonia Gurgone:** Writing – original draft, Visualization, Validation, Methodology, Investigation, Formal analysis, Data curation, Conceptualization. **Elisabetta Ciani:** Writing – original draft, Supervision, Data curation. **Riccardo Pizzo:** Writing – original draft, Visualization, Validation, Methodology, Investigation, Formal analysis, Data curation, Conceptualization. **Tommaso Pizzorusso:** Writing – original draft, Supervision, Data curation. **Alessandra Raspanti:** Writing – original draft, Visualization, Validation, Methodology, Investigation, Formal analysis, Data curation, Conceptualization. **Francesco Ferrini:** Writing – original draft, Investigation, Formal analysis, Data curation. **Giorgio Medici:** Investigation. **Debora Comai:** Investigation. **Lamprini Katsanou:** Investigation.

Fundings

#NEXTGENERATIONEU (NGEU), Ministry of University and Research (MUR), National Recovery and Resilience Plan (NRRP), project MNESYS (PE0000006) – A Multiscale integrated approach to the study of the nervous system in health and disease (DN. 1553 11.10.2022) to E. C.; Tuscany Health Ecosystem (THE) Project (CUP I53C22000780001), National Recovery and Resilience Plan (NRPP), within the NextGeneration Europe (NGEU) Program; the CRONOLAB project of the PRO3 joint program; and PRIN2017 2017HMH8FA and 20228RMXBE to T.P.; Fondazione Cassa di Risparmio di Torino (grant 2015.1690) to F.F.; International Foundation for CDKL5 Research (USA), Albero di Greta CDKL5 (Italy), CDKL5 Insieme Verso la Cura (Italy), Fondazione Cassa di Risparmio di Torino (Italy, grant n. 2018.0889), Association Française du Syndrome de Rett (n. 2017–05) to M.G., National Recovery and Resilience Plan (NRPP) within the NextGeneration Europe (NGEU) Program PRIN P2022N2B7E - CUP D53D23012250006, and Fondazione Telethon-Italy (n. GGP19045) to E.C. and M.G. This study is part of the MIUR Project "Dipartimenti di Eccellenza" of the Rita Levi-Montalcini Department of Neuroscience (University of Turin).

Declaration of Competing Interest

The authors declare that they have no known competing financial interests or personal relationships that could have appeared to influence the work reported in this paper

Appendix A. Supporting information

Supplementary data associated with this article can be found in the online version at doi:10.1016/j.pneurobio.2026.102949.

References

Amendola, E., Zhan, Y., Mattucci, C., Castroflorio, E., Calcagno, E., Fuchs, C., Lonetti, G., Silingardi, D., Vyssotski, A.L., Farley, D., Ciani, E., Pizzorusso, T., Giustetto, M., Gross, C.T., 2014. Mapping pathological phenotypes in a mouse model of CDKL5 disorder. PLoS. One 9 (5), e91613. https://doi.org/10.1371/journal.pone.0091613.

Antón-Bolaños, N., Sempere-Ferràndez, A., Guillamón-Vivancos, T., Martini, F.J., Pérez-Saiz, L., Gezelius, H., Filipchuk, A., Valdeolmillos, M., López-Bendito, G., 2019. Prenatal activity from thalamic neurons governs the emergence of functional cortical maps in mice. Science 364 (6444), 987–990. https://doi.org/10.1126/science.aav7617.

Arakawa, H., Erzurumlu, R.S., 2015. Role of whiskers in sensorimotor development of C57BL/6 mice. Behav. Brain Res. 287, 146–155. https://doi.org/10.1016/j.bbr.2015.03.040.

Balasco, L., Pagani, M., Pangrazzi, L., Chelini, G., Viscido, F., Chama, A.G.C., Galbusera, A., Provenzano, G., Gozzi, A., Bozzi, Y., 2022. Somatosensory cortex hyperconnectivity and impaired whisker-dependent responses in Cntnap2-/- mice. Neurobiol. Dis. 169, 105742. https://doi.org/10.1016/j.nbd.2022.105742.

Ballester-Rosado, C.J., Sun, H., Huang, J.Y., Lu, H.C., 2016. mGluR5 exerts cell-autonomous influences on the functional and anatomical development of layer IV cortical neurons in the mouse primary somatosensory cortex. J. Neurosci. 36 (34), 8802–8814. https://doi.org/10.1523/JNEUROSCI.1224-16.2016.

Baltussen, L.L., Negraes, P.D., Silvestre, M., Claxton, S., Moeskops, M., Christodoulou, E., Flynn, H.R., Snijders, A.P., Muotri, A.R., Ultanir, S.K., 2018. Chemical genetic

identification of CDKL5 substrates reveals its role in neuronal microtubule dynamics. EMBO J. 37 (24), e99763. https://doi.org/10.15252/embj.201899763.
Baronio, D., Castro, K., Gonchoroski, T., de Melo, G.M., Nunes, G.D., Bambini-Junior, V., Gottfried, C., Riesgo, R., 2015. Effects of an H3R antagonist on the animal model of autism induced by prenatal exposure to valproic acid. PLoS. One 10 (1), e0116363. https://doi.org/10.1371/journal.pone.0116363.
Baum, S.H., Stevenson, R.A., Wallace, M.T., 2015. Behavioral, perceptual, and neural alterations in sensory and multisensory function in autism spectrum disorder. Prog. Neurobiol. 134, 140–160. https://doi.org/10.1016/j.pneurobio.2015.09.007.
Berardi, N., Pizzorusso, T., Maffei, L., 2004. Extracellular matrix and visual cortical plasticity: freeing the synapse. Neuron 44 (6), 905–908. https://doi.org/10.1016/j.neuron.2004.12.008.
Bhattacherjee, A., Winter, M.K., Eggimann, L.S., Mu, Y., Gunewardena, S., Liao, Z., Christianson, J.A., Smith, P.G., 2017. Motor, somatosensory, viscerosensory and metabolic impairments in a heterozygous female rat model of Rett syndrome. Int. J. Mol. Sci. 19 (1), 97. https://doi.org/10.3390/ijms19010097.
Boyd, B.A., Baranek, G.T., Sideris, J., Poe, M.D., Watson, L.R., Patten, E., Miller, H., 2010. Sensory features and repetitive behaviors in children with autism and developmental delays. Autism Res. 3 (2), 78–87. https://doi.org/10.1002/aur.124.
Cang, J., Kalatsky, V.A., Löwel, S., Stryker, M.P., 2005. Optical imaging of the intrinsic signal as a measure of cortical plasticity in the mouse. Vis. Neurosci. 22 (5), 685–691. https://doi.org/10.1017/S0952523805225178.
Chapleau, C.A., Boggio, E.M., Calfa, G., Percy, A.K., Giustetto, M., Pozzo-Miller, L., 2012. Hippocampal CA1 pyramidal neurons of Mecp2 mutant mice show a dendritic spine phenotype only in the presymptomatic stage. Neural Plast., 976164 https://doi.org/10.1155/2012/976164.
Chen, Q., Deister, C.A., Gao, X., et al., 2020. Dysfunction of cortical GABAergic neurons leads to sensory hyper-reactivity in a *Shank3* mouse model of ASD. Nat. Neurosci. 23, 520–532. https://doi.org/10.1038/s41593-020-0598-6.
Chen, P., Hong, W., 2018. Neural circuit mechanisms of social behavior. Neuron 98 (1), 16–30. https://doi.org/10.1016/j.neuron.2018.02.026.
Cheung, P.P.P., Lau, B.W.M., 2020. Neurobiology of sensory processing in autism spectrum disorder. Prog. Mol. Biol. Transl. Sci. 173, 161–181. https://doi.org/10.1016/bs.pmbts.2020.04.020.
Ciccarelli, A., Calza, A., Santoru, F., Grasso, F., Concas, A., Sassoè-Pognetto, M., Giustetto, M., 2013. Morphine withdrawal produces ERK-dependent and ERK-independent epigenetic marks in neurons of the nucleus accumbens and lateral septum. Neuropharmacology 70, 168–179. https://doi.org/10.1016/j.neuropharm.2012.12.010.
Concina, G., Gurgone, A., Boggio, E.M., Raspanti, A., Pizzo, R., Morello, N., Castroflorio, E., Pizzorusso, T., Sacchetti, B., Giustetto, M., 2023. Stabilizing immature dendritic spines in the auditory cortex: a key mechanism for mTORC1-mediated enhancement of long-term fear memories. J. Neurosci. 43 (50), 8744–8755. https://doi.org/10.1523/JNEUROSCI.0204-23.2023.
Corbetta, D., Snapp-Childs, W., 2009. Seeing and touching: the role of sensory-motor experience on the development of infant reaching. Infant. Behav. Dev. 32 (1), 44–58. https://doi.org/10.1016/j.infbeh.2008.10.004.
Datwani, A., Iwasato, T., Itohara, S., Erzurumlu, R.S., 2002. NMDA receptor-dependent pattern transfer from afferents to postsynaptic cells and dendritic differentiation in the barrel cortex. Mol. Cell. Neurosci. 21 (3), 477–492. https://doi.org/10.1006/mcne.2002.1195.
Della Sala, G., Putignano, E., Chelini, G., Melani, R., Calcagno, E., Michele Ratto, G., Amendola, E., Gross, C.T., Giustetto, M., Pizzorusso, T., 2016. Dendritic spine instability in a mouse model of CDKL5 disorder is rescued by Insulin-like Growth Factor 1. Biol. Psychiatry 80 (4), 302–311. https://doi.org/10.1016/j.biopsych.2015.08.028.
Erzurumlu, R.S., Gaspar, P., 2012. Development and critical period plasticity of the barrel cortex. Eur. J. Neurosci. 35 (10), 1540–1553. https://doi.org/10.1111/j.1460-9568.2012.08075.x.
Erzurumlu, R.S., Gaspar, P., 2020. How the barrel cortex became a working model for developmental plasticity: a historical perspective. J. Neurosci. 40 (34), 6460–6473. https://doi.org/10.1523/JNEUROSCI.0582-20.2020.
Estes, A., Zwaigenbaum, L., Gu, H., St John, T., Paterson, S., Elison, J.T., Hazlett, H., Botteron, K., Dager, S.R., Schultz, R.T., Kostopoulos, P., Evans, A., Dawson, G., Eliason, J., Alvarez, S., Piven, J., network, I.B.I.S., 2015. Behavioral, cognitive, and adaptive development in infants with autism spectrum disorder in the first 2 years of life. J. Neurodev. Disord. 7 (1), 24. https://doi.org/10.1186/s11689-015-9117-6.
Feldmeyer, D., 2012. Excitatory neuronal connectivity in the barrel cortex. Front. Neuroanat. 6, 24. https://doi.org/10.3389/fnana.2012.00024.
Fong, S.S., Tsang, W.W., Ng, G.Y., 2012. Altered postural control strategies and sensory organization in children with developmental coordination disorder. Hum. Mov. Sci. 31 (5), 1317–1327. https://doi.org/10.1016/j.humov.2011.11.003.
Gennaccaro, L., Fuchs, C., Loi, M., Pizzo, R., Alvente, S., Berteotti, C., Lupori, L., Sagona, G., Galvani, G., Gurgone, A., Raspanti, A., Medici, G., Tassinari, M., Trazzi, S., Ren, E., Rimondini, R., Pizzorusso, T., Zoccoli, G., Giustetto, M., Ciani, E., 2021. Age-related cognitive and motor decline in a mouse model of CDKL5 Deficiency Disorder is associated with increased neuronal senescence and death. Aging Dis. 12 (3), 764–785. https://doi.org/10.14336/AD.2020.0827.
Geuze, R.H., 2003. Static balance and developmental coordination disorder. Hum. Mov. Sci. 22 (4–5), 527–548. https://doi.org/10.1016/j.humov.2003.09.008.
Giese, K.P., 2021. The role of CaMKII autophosphorylation for NMDA receptor-dependent synaptic potentiation. Neuropharmacology 193, 108616. https://doi.org/10.1016/j.neuropharm.2021.108616.
Goddard-Blythe, S., 2000. Early learning in the balance: priming the first ABC. Supp Learn. 15, 154–158. https://doi.org/10.1111/1467-9604.00168.
Goddard-Blythe, S.A., 2011. Neuromotor maturity as an indicator of developmental readiness for Education. In: Kulesza, E.M. (Ed.), Movement, vision, hearing – the basis of learning. Wydawnictwo APS, Warsaw.
Grzadzinski, R., Janvier, D., Kim, S.H., 2020. Recent developments in treatment outcome measures for young children with Autism Spectrum Disorder (ASD). Semin. Pediatr. Neurol. 34, 100806. https://doi.org/10.1016/j.spen.2020.100806.
Gurgone, A., Pizzo, R., Raspanti, A., Chiantia, G., Devi, S., Comai, D., Morello, N., Pilotto, F., Gnavi, S., Lupori, L., Mazziotti, R., Sagona, G., Putignano, E., Nocentini, A., Supuran, C.T., Marcantoni, A., Pizzorusso, T., Giustetto, M., 2023. mGluR5 PAMs rescue cortical and behavioural defects in a mouse model of CDKL5 Deficiency Disorder. Neuropsychopharmacology 48 (6), 877–886. https://doi.org/10.1038/s41386-022-01412-3.
Han, Q., Kim, Y.H., Wang, X., Liu, D., Zhang, Z.J., Bey, A.L., Lay, M., Chang, W., Berta, T., Zhang, Y., Jiang, Y.H., Ji, R.R., 2016. SHANK3 deficiency impairs heat hyperalgesia and TRPV1 signaling in primary sensory neurons. Neuron 92 (6), 1279–1293. https://doi.org/10.1016/j.neuron.2016.11.007.
Hanuska, A., Ribiczey, P., Kató, E., Papp, Z.T., Varga, Z.V., Giricz, Z., Tóth, Z.E., Könczöl, K., Zsembery, Á., Zelles, T., Harsing Jr, L.G., Köles, L., 2024. Potentiation of NMDA receptors by AT1 angiotensin receptor activation in layer V pyramidal neurons of the rat prefrontal cortex. Int. J. Mol. Sci. 25 (23), 12644. https://doi.org/10.3390/ijms252312644.
He, C.X., Cantu, D.A., Mantri, S.S., Zeiger, W.A., Goel, A., Portera-Cailliau, C., 2017. Tactile defensiveness and impaired adaptation of neuronal activity in the Fmr1 knock-out mouse model of autism. J. Neurosci. 37 (27), 6475–6487. https://doi.org/10.1523/JNEUROSCI.0651-17.2017.
Heimel, J.A., Hartman, R.J., Hermans, J.M., Levelt, C.N., 2007. Screening mouse vision with intrinsic signal optical imaging. Eur. J. Neurosci. 25 (3), 795–804. https://doi.org/10.1111/j.1460-9568.2007.05333.x.
Hensch, T.K., 2005. Critical period plasticity in local cortical circuits. Nat. Rev. Neurosci. 6 (11), 877–888. https://doi.org/10.1038/nrn1787.
Hertenstein, M.J., Verkamp, J.M., Kerestes, A.M., Holmes, R.M., 2006. The communicative functions of touch in humans, nonhuman primates, and rats: a review and synthesis of the empirical research. Genet. Soc. Gen. Psychol. Monogr. 132 (1), 5–94. https://doi.org/10.3200/mono.132.1.5-94.
Huang, J.Y., Lu, H.C., 2018. mGluR5 tunes NGF/TrkA signaling to orient spiny stellate neuron dendrites toward thalamocortical axons during whisker-barrel map formation. Cereb. Cortex 28 (6), 1991–2006. https://doi.org/10.1093/cercor/bhx105.
Hubel, D.H., Wiesel, T.N., 1970. The period of susceptibility to the physiological effects of unilateral eye closure in kittens. J. Physiol. 206 (2), 419–436. https://doi.org/10.1113/jphysiol.1970.sp009022.
Iwasato, T., Datwani, A., Wolf, A.M., Nishiyama, H., Taguchi, Y., Tonegawa, S., Knöpfel, T., Erzurumlu, R.S., Itohara, S., 2000. Cortex-restricted disruption of NMDAR1 impairs neuronal patterns in the barrel cortex. Nature 406 (6797), 726–731. https://doi.org/10.1038/35021059.
Jakimiec, M., Paprocka, J., Śmigiel, R., 2020. CDKL5 Deficiency Disorder- A complex epileptic encephalopathy. Brain Sci. 10 (2), 107. https://doi.org/10.3390/brainsci10020107.
Jhang, C.L., Huang, T.N., Hsueh, Y.P., Liao, W., 2017. Mice lacking cyclin-dependent kinase-like 5 manifest autistic and ADHD-like behaviors. Hum. Mol. Genet. 26 (20), 3922–3934. https://doi.org/10.1093/hmg/ddx279.
Kennedy, M.B., 2013. Synaptic Signaling in Learning and Memory. Cold Spring Harb. Perspect. Biol. 8 (2), a016824. https://doi.org/10.1101/cshperspect.a016824.
Kim, J.Y., Grunke, S.D., Levites, Y., Golde, T.E., Jankowsky, J.L., 2014. Intracerebroventricular viral injection of the neonatal mouse brain for persistent and widespread neuronal transduction. J. Vis. Exp. 91, 51863. https://doi.org/10.3791/51863.
Knudsen, E.I., 2004. Sensitive periods in the development of the brain and behavior. J. Cogn. Neurosci. 16 (8), 1412–1425. https://doi.org/10.1162/0898929042304796.
Krapivinsky, G., Krapivinsky, L., Manasian, Y., Ivanov, A., Tyzio, R., Pellegrino, C., Ben-Ari, Y., Clapham, D.E., Medina, I., 2003. The NMDA receptor is coupled to the ERK pathway by a direct interaction between NR2B and RasGRF1. Neuron 40 (4), 775–784. https://doi.org/10.1016/s0896-6273(03)00645-7.
Lauer, S.M., Schneeweiß, U., Brecht, M., Ray, S., 2018. Visualization of cortical modules in flattened mammalian cortices. J. Vis. Exp. (131),, 56992. https://doi.org/10.3791/56992.
Li, H., Crair, M.C., 2011. How do barrels form in somatosensory cortex? Ann. N. Y Acad. Sci. 1225, 119–129. https://doi.org/10.1111/j.1749-6632.2011.06024.x.
Liao, W., Lee, K.Z., 2023. CDKL5-mediated developmental tuning of neuronal excitability and concomitant regulation of transcriptome. Hum. Mol. Genet. 32 (23), 3276–3298. https://doi.org/10.1093/hmg/ddad149.
Lisman, J., Yasuda, R., Raghavachari, S., 2012. Mechanisms of CaMKII action in long-term potentiation. Nat. Rev. Neurosci. 13 (3), 169–182. https://doi.org/10.1038/nrn3192.
Lupori, L., Sagona, G., Fuchs, C., Mazziotti, R., Stefanov, A., Putignano, E., Napoli, D., Strettoi, E., Ciani, E., Pizzorusso, T., 2019. Site-specific abnormalities in the visual system of a mouse model of CDKL5 Deficiency Disorder. Hum. Mol. Genet. 28 (17), 2851–2861. https://doi.org/10.1093/hmg/ddz102.
Mazziotti, R., Lupori, L., Sagona, G., Gennaro, M., Della Sala, G., Putignano, E., Pizzorusso, T., 2017. Searching for biomarkers of CDKL5 disorder: early-onset visual impairment in CDKL5 mutant mice. Hum. Mol. Genet. 26 (12), 2290–2298. https://doi.org/10.1093/hmg/ddx119.
McFarlane, H.G., Kusek, G.K., Yang, M., Phoenix, J.L., Bolivar, V.J., Crawley, J.N., 2008. Autism-like behavioral phenotypes in BTBR T+tf/J mice. Genes Brain Behav. 7 (2), 152–163. https://doi.org/10.1111/j.1601-183X.2007.00330.x.

Medici, G., Tassinari, M., Galvani, G., Bastianini, S., Gennaccaro, L., Loi, M., Mottolese, N., Alvente, S., Berteotti, C., Sagona, G., Lupori, L., Candini, G., Baggett, H.R., Zoccoli, G., Giustetto, M., Muotri, A., Pizzorusso, T., Nakai, H., Trazzi, S., Ciani, E., 2022. Expression of a secretable, cell-penetrating CDKL5 protein enhances the efficacy of gene therapy for CDKL5 Deficiency Disorder. Neurotherapeutics 19 (6), 1886–1904. https://doi.org/10.1007/s13311-022-01295-8.

Mikkelsen, M., Wodka, E.L., Mostofsky, S.H., Puts, N.A.J., 2018. Autism spectrum disorder in the scope of tactile processing. Dev. Cogn. Neurosci. 29, 140–150. https://doi.org/10.1016/j.dcn.2016.12.005.

Mizuno, H., Luo, W., Tarusawa, E., Saito, Y.M., Sato, T., Yoshimura, Y., Itohara, S., Iwasato, T., 2014. NMDAR-regulated dynamics of layer 4 neuronal dendrites during thalamocortical reorganization in neonates. Neuron 82 (2), 365–379. https://doi.org/10.1016/j.neuron.2014.02.026.

Mizuno, H., Rao, M.S., Mizuno, H., Sato, T., Nakazawa, S., Iwasato, T., 2021. NMDA receptor enhances correlation of spontaneous activity in neonatal barrel cortex. J. Neurosci. 41 (6), 1207–1217. https://doi.org/10.1523/JNEUROSCI.0527-20.2020.

Nakagawa, N., Iwasato, T., 2023. Golgi polarity shift instructs dendritic refinement in the neonatal cortex by mediating NMDA receptor signaling. Cell. Rep. 42 (8), 112843. https://doi.org/10.1016/j.celrep.2023.112843.

Narboux-Nême, N., Evrard, A., Ferezou, I., Erzurumlu, R.S., Kaeser, P.S., Lainé, J., Rossier, J., Ropert, N., Südhof, T.C., Gaspar, P., 2012. Neurotransmitter release at the thalamocortical synapse instructs barrel formation but not axon patterning in the somatosensory cortex. J. Neurosci. : Off. J. Soc. Neurosci. 32 (18), 6183–6196. https://doi.org/10.1523/JNEUROSCI.0343-12.2012.

Okuda, K., Kobayashi, S., Fukaya, M., Watanabe, A., Murakami, T., Hagiwara, M., Sato, T., Ueno, H., Ogonuki, N., Komano-Inoue, S., Manabe, H., Yamaguchi, M., Ogura, A., Asahara, H., Sakagami, H., Mizuguchi, M., Manabe, T., Tanaka, T., 2017. CDKL5 controls postsynaptic localization of GluN2B-containing NMDA receptors in the hippocampus and regulates seizure susceptibility. Neurobiol. Dis. 106, 158–170. https://doi.org/10.1016/j.nbd.2017.07.002.

Orefice, L.L., Mosko, J.R., Morency, D.T., Wells, M.F., Tasnim, A., Mozeika, S.M., Ye, M., Chirila, A.M., Emanuel, A.J., Rankin, G., Fame, R.M., Lehtinen, M.K., Feng, G., Ginty, D.D., 2019. Targeting Peripheral Somatosensory Neurons to Improve Tactile-Related Phenotypes in ASD Models. Cell 178 (4), 867–886.e24. https://doi.org/10.1016/j.cell.2019.07.024.

Orefice, L.L., Zimmerman, A.L., Chirila, A.M., Sleboda, S.J., Head, J.P., Ginty, D.D., 2016. Peripheral Mechanosensory Neuron Dysfunction Underlies Tactile and Behavioral Deficits in Mouse Models of ASDs. Cell 166 (2), 299–313. https://doi.org/10.1016/j.cell.2016.05.033.

Parfrey, K., Gibbons, S.G., Drinkwater, E.J., Behm, D.G., 2014. Effect of head and limb orientation on trunk muscle activation during abdominal hollowing in chronic low back pain. BMC Musculoskelet. Disord. 15, 52. https://doi.org/10.1186/1471-2474-15-52.

Patil, O., Kaple, M., 2023. Sensory Processing Differences in Individuals With Autism Spectrum Disorder: A Narrative Review of Underlying Mechanisms and Sensory-Based Interventions. Cureus 15 (10), e48020. https://doi.org/10.7759/cureus.48020.

Petersen, C.C.H., 2019. Sensorimotor processing in the rodent barrel cortex. Nat. rev. Neurosci. 20 (9), 533–546. https://doi.org/10.1038/s41583-019-0200-y.

Pizzo, R., Gurgone, A., Castroflorio, E., Amendola, E., Gross, C., Sassoè-Pognetto, M., Giustetto, M., 2016. Lack of Cdkl5 Disrupts the Organization of Excitatory and Inhibitory Synapses and Parvalbumin Interneurons in the Primary Visual Cortex. Front. Cell. Neurosci. 10, 261. https://doi.org/10.3389/fncel.2016.00261.

Pizzo, R., Lamarca, A., Sassoè-Pognetto, M., Giustetto, M., 2020. Structural Bases of Atypical Whisker Responses in a Mouse Model of CDKL5 Deficiency Disorder. Neuroscience 445, 130–143. https://doi.org/10.1016/j.neuroscience.2019.08.033.

Riemersma, I.W., Ike, K.G.O., Sollie, T., Meijer, E.L., Havekes, R., Kas, M.J.H., 2024. Suppression of Cofilin function in the somatosensory cortex alters social contact behavior in the BTBR mouse inbred line. Cereb. Cortex 34 (4). https://doi.org/10.1093/cercor/bhae136.

Robertson, C.E., Baron-Cohen, S., 2017. Sensory perception in autism. Nat. Rev. Neurosci. 18 (11), 671–684. https://doi.org/10.1038/nrn.2017.112.

Rusconi, L., Salvatoni, L., Giudici, L., Bertani, I., Kilstrup-Nielsen, C., Broccoli, V., Landsberger, N., 2008. CDKL5 expression is modulated during neuronal development and its subcellular distribution is tightly regulated by the C-terminal tail. J. Biol. Chem. 283 (44), 30101–30111. https://doi.org/10.1074/jbc.M804613200.

Sacrey, L.R., Zwaigenbaum, L., Bryson, S., Brian, J., Smith, I.M., Raza, S., Roberts, W., Szatmari, P., Vaillancourt, T., Roncadin, C., Garon, N., 2019. Developmental trajectories of adaptive behavior in autism spectrum disorder: a high-risk sibling cohort. J. Child Psychol. Psychiatry Allied Discip. 60 (6), 697–706. https://doi.org/10.1111/jcpp.12985.

Song, X., Xia, Z., Martinez, D., Xu, B., Spritzer, Z., Zhang, Y., Nugent, E., Ho, Y., Terzic, B., Zhou, Z., 2025. Independent genetic strategies define the scope and limits of CDKL5 deficiency disorder reversal. Cell Rep. Med. 6 (2), 101926. https://doi.org/10.1016/j.xcrm.2024.101926.

Stagni, F., Raspanti, A., Giacomini, A., Guidi, S., Emili, M., Ciani, E., Giuliani, A., Bighinati, A., Calzà, L., Magistretti, J., Bartesaghi, R., 2017. Long-term effect of neonatal inhibition of APP gamma-secretase on hippocampal development in the Ts65Dn mouse model of Down syndrome. Neurobiol. Dis. 103, 11–23. https://doi.org/10.1016/j.nbd.2017.03.012.

Staiger, J.F., Petersen, C.C.H., 2021. Neuronal Circuits in Barrel Cortex for Whisker Sensory Perception. Physiol. Rev. 101 (1), 353–415. https://doi.org/10.1152/physrev.00019.2019.

Sullivan, R.M., Landers, M.S., Flemming, J., Vaught, C., Young, T.A., Jonathan Polan, H., 2003. Characterizing the functional significance of the neonatal rat vibrissae prior to the onset of whisking. Somatosens. Mot. Res. 20 (2), 157–162. https://doi.org/10.1080/0899022031000105190.

Tang, S., Terzic, B., Wang, I.J., Sarmiento, N., Sizov, K., Cui, Y., Takano, H., Marsh, E.D., Zhou, Z., Coulter, D.A., 2019. Altered NMDAR signaling underlies autistic-like features in mouse models of CDKL5 deficiency disorder. Nat. Commun. 10 (1), 2655. https://doi.org/10.1038/s41467-019-10689-w.

Tărlungeanu, D.C., Deliu, E., Dotter, C.P., Kara, M., Janiesch, P.C., Scalise, M., Galluccio, M., Tesulov, M., Morelli, E., Sonmez, F.M., Bilguvar, K., Ohgaki, R., Kanai, Y., Johansen, A., Esharif, S., Ben-Omran, T., Topcu, M., Schlessinger, A., Indiveri, C., Duncan, K.E., Caglayan, A.O., Gunel, M., Gleeson, J.G., Novarino, G., 2016. Impaired Amino Acid Transport at the Blood Brain Barrier Is a Cause of Autism Spectrum Disorder. Cell 167 (6), 1481–1494.e18. https://doi.org/10.1016/j.cell.2016.11.013.

Tassinari, M., Uguagliati, B., Trazzi, S., Cerchier, C.B., Cavina, O.V., Mottolese, N., Loi, M., Candini, G., Medici, G., Ciani, E., 2023. Early-onset brain alterations during postnatal development in a mouse model of CDKL5 deficiency disorder. Neurobiol. Dis. 182, 106146. https://doi.org/10.1016/j.nbd.2023.106146.

Teitelbaum, O., Benton, T., Shah, P.K., Prince, A., Kelly, J.L., Teitelbaum, P., 2004. Eshkol-Wachman movement notation in diagnosis: the early detection of Asperger's syndrome. Proc. Natl. Acad. Sci. USA 101 (32), 11909–11914. https://doi.org/10.1073/pnas.0403919101.

Terzic, B., Davatolhagh, M.F., Ho, Y., Tang, S., Liu, Y.T., Xia, Z., Cui, Y., Fuccillo, M.V., Zhou, Z., 2021. Temporal manipulation of Cdkl5 reveals essential postdevelopmental functions and reversible CDKL5 deficiency disorder-related deficits. J. Clin. Investig. 131 (20), e143655. https://doi.org/10.1172/JCI143655.

Turner-Brown, L.M., Baranek, G.T., Reznick, J.S., Watson, L.R., Crais, E.R., 2013. The First Year Inventory: a longitudinal follow-up of 12-month-old to 3-year-old children. Autism : Int. J. Res. Pract. 17 (5), 527–540. https://doi.org/10.1177/1362361312439633.

Van Bergen, N.J., Massey, S., Quigley, A., Rollo, B., Harris, A.R., Kapsa, R.M.I., Christodoulou, J., 2022. CDKL5 deficiency disorder: molecular insights and mechanisms of pathogenicity to fast-track therapeutic development. Biochem. Soc. trans. 50 (4), 1207–1224. https://doi.org/10.1042/BST20220791.

Vigli, D., Rusconi, L., Valenti, D., La Montanara, P., Cosentino, L., Lacivita, E., Leopoldo, M., Amendola, E., Gross, C., Landsberger, N., Laviola, G., Kilstrup-Nielsen, C., Vacca, R.A., De Filippis, B., 2019. Rescue of prepulse inhibition deficit and brain mitochondrial dysfunction by pharmacological stimulation of the central serotonin receptor 7 in a mouse model of CDKL5 Deficiency Disorder. Neuropharmacology 144, 104–114. https://doi.org/10.1016/j.neuropharm.2018.10.018.

Vitali, I., Jabaudon, D., 2014. Synaptic biology of barrel cortex circuit assembly. Semin. Cell Dev. Biol. 35, 156–164. https://doi.org/10.1016/j.semcdb.2014.07.009 2014.

Vitalis, T., Dauphinot, L., Gressens, P., Potier, M.C., Mariani, J., Gaspar, P., 2018. RORα Coordinates Thalamic and Cortical Maturation to Instruct Barrel Cortex Development. Cereb Cortex. 28 (11), 3994–4007.

Wang, I.T., Allen, M., Goffin, D., Zhu, X., Fairless, A.H., Brodkin, E.S., Siegel, S.J., Marsh, E.D., Blendy, J.A., Zhou, Z., 2012. Loss of CDKL5 disrupts kinome profile and event-related potentials leading to autistic-like phenotypes in mice. Proc Natl Acad Sci U S A. 109 (52), 21516–21521. https://doi.org/10.1073/pnas.1216988110.

Wang, C.F., Hsing, H.W., Zhuang, Z.H., Wen, M.H., Chang, W.J., Briz, C.G., Nieto, M., Shyu, B.C., Chou, S.J., 2017. Lhx2 Expression in Postmitotic Cortical Neurons Initiates Assembly of the Thalamocortical Somatosensory Circuit. Cell Rep. 18 (4), 849–856. https://doi.org/10.1016/j.celrep.2017.01.001.

Wirkner, K., Günther, A., Weber, M., Guzman, S.J., Krause, T., Fuchs, J., Köles, L., Nörenberg, W., Illes, P., 2007. Modulation of NMDA receptor current in layer V pyramidal neurons of the rat prefrontal cortex by P2Y receptor activation. Cereb. Cortex 17 (3), 621–631. https://doi.org/10.1093/cercor/bhk012 (New York, N.Y. : 1991).

Wirkner, K., Köles, L., Thümmler, S., Luthardt, J., Poelchen, W., Franke, H., Fürst, S., Illes, P., 2002. Interaction between P2Y and NMDA receptors in layer V pyramidal neurons of the rat prefrontal cortex. Neuropharmacology 42 (4), 476–488. https://doi.org/10.1016/s0028-3908(01)00199-x.

Wolff, J.J., Dimian, A.F., Botteron, K.N., Dager, S.R., Elison, J.T., Estes, A.M., Hazlett, H. C., Schultz, R.T., Zwaigenbaum, L., Piven, J., 2019. A longitudinal study of parent-reported sensory responsiveness in toddlers at-risk for autism. J. Child Psychol. Psychiatry Allied Discip. 60 (3), 314–324. https://doi.org/10.1111/jcpp.12978.

Wu, C.S., Ballester Rosado, C.J., Lu, H.C., 2011. What can we get from 'barrels': the rodent barrel cortex as a model for studying the establishment of neural circuits. Eur. J. Neurosci. 34 (10), 1663–1676. https://doi.org/10.1111/j.1460-9568.2011.07892.x.

Yang, J.W., Kilb, W., Kirischuk, S., Unichenko, P., Stüttgen, M.C., Luhmann, H.J., 2018. Development of the whisker-to-barrel cortex system. Curr. Opin. Neurobiol. 53, 29–34. https://doi.org/10.1016/j.conb.2018.04.023.

Yennawar, M., White, R.S., Jensen, F.E., 2019. AMPA Receptor Dysregulation and Therapeutic Interventions in a Mouse Model of CDKL5 Deficiency Disorder. J. Neurosci. : Off. J. Soc. Neurosci. 39 (24), 4814–4828. https://doi.org/10.1523/JNEUROSCI.2041-18.2019.

Young, T.R., Yamamoto, M., Kikuchi, S.S., Yoshida, A.C., Abe, T., Inoue, K., Johansen, J. P., Benucci, A., Yoshimura, Y., Shimogori, T., 2023. Thalamocortical control of cell-type specificity drives circuits for processing whisker-related information in mouse

barrel cortex. Nat. Commun. 14 (1), 6077. https://doi.org/10.1038/s41467-023-41749-x.
Zafeiriou, D.I., 2004. Primitive reflexes and postural reactions in the neurodevelopmental examination. Pediatr. Neurol. 31 (1), 1–8. https://doi.org/10.1016/j.pediatrneurol.2004.01.012.
Zhu, Y.C., Xiong, Z.Q., 2019. Molecular and Synaptic Bases of CDKL5 Disorder. Dev. Neurobiol. 79 (1), 8–19. https://doi.org/10.1002/dneu.22639.